Journal of Neuroimmunology 331 (2019) 58–73

Contents lists available at ScienceDirect

Journal of Neuroimmunology

journal homepage: www.elsevier.com/locate/jneuroim

TLR4 in circumventricular neural stem cells is a negative regulator for thermogenic pathways in the mouse brain

Shiori Muneoka[a], Saki Murayama[a], Yousuke Nakano[a,c], Seiji Miyata[a,b,*]

[a] Department of Applied Biology, Japan
[b] The Center for Advanced Insect Research Promotion (CAIRP), Kyoto Institute of Technology, Matsugasaki, Sakyo-ku, Kyoto 606-8585, Japan
[c] Department of Anatomy and Brain Science, Kansai Medical University, Hirakata, Japan

ARTICLE INFO

Keywords:
Inflammation
Circumventricular organs
Fever
NF-κB
Fos

ABSTRACT

Toll-like receptor 4 (TLR4) recognizes bacteria-derived lipopolysaccharide (LPS). In the present study, we found that intraperitoneal LPS activated nuclear factor-κ B (NF-κB) in TLR4-expressing neural stem cells (NSCs) in the circumventricular brain regions of mice. Intracerebroventricular preadministration of low-dose TLR4 inhibitors significantly augmented hyperthermia together with the inhibition of NF-κB activation in circumventricular NSCs of LPS-inflamed animals. Moreover, intracerebroventricular administration of high-dose TLR4 inhibitors induced hyperthermia and Fos activation in circumventricular NSCs and hypothalamic neurons. These results suggest that TLR4 on circumventricular NSCs functions as a central regulator for thermogenesis under inflamed and normal conditions.

1. Introduction

Recognition of infection is the first and most important process required to initiate proper physiological responses to fight infection. The recognition of pathogens is mediated by several classes of receptors collectively referred to as pattern-recognition receptors, of which Toll-like receptors (TLRs) are the most widely studied (McCusker and Kelley, 2013; Gay et al., 2014). The reaction to lipopolysaccharide (LPS) derived from Gram-negative bacteria, which triggers severe inflammation by activating TLR4, is the best-characterized experimental inflammatory system of bacterial infection. Administration of LPS leads to acute biological activity, including changes in body temperature, autonomic responses, anorexia, adipsia, modifications of sleep patterns, and decreases in locomotor activity (Roth et al., 2004; Rivest, 2003). Systemic low-dose LPS activates TLR4 to trigger inflammatory responses and hyperthermia, which allows host animals to respond to invading pathogens, whereas excessive LPS leads to the development of sepsis and hypothermia (Ramachandran, 2014).

LPS is able to bind with CD14 only in the presence of LPS-binding protein, and the complex of LPS-proteins is then able to interact with TLR4. The activation of TLR4 leads to a series of signaling cascades that result in the activation of two distinct signaling pathways: nuclear factor-κB (NF-κB) and activator protein-1 (Takeda and Akira, 2004; Rivest, 2003). The trimer consisting of a NF-κB dimer and monomeric inhibitor of κB (IκBα) is present in the cytosol in an inactivated state, whereas the NF-κB dimer is translocated into the nucleus after dissociation of IκBα (Perkins, 2007), and thereafter binds to the NF-κB motif of DNA to transcribe proinflammatory genes such as tumor necrosis factor (TNF)-α, interleukin (IL)-1β, and IL-6 (Brasier, 2010). Activator protein-1 is also known to control the expression of numerous cytokines (Adcock, 1997). The cytokines IL-1β and IL-6 activate cyclooxygenase-2 (COX-2) via the production of prostaglandin E2 (PGE2) to induce inflammatory and thermoregulatory responses (Conti et al., 2004). The selective loss of the neuronal PGE2 receptor in the preoptic area (POA) prevents PGE2- and LPS-induced hyperthermia (Lazarus et al., 2007). Selective gene deletion of PGE2-synthesizing enzymes in brain endothelial cells attenuates hyperthermia (Wilhelms et al., 2014). Hyperthermic response is dependent on PGE2 synthesis by endothelial

Abbreviations: AH, anterior hypothalamic area; AP, area postrema; Arc, arcuate nucleus; BBB, blood-brain barrier; CC, central canal; CVOs, circumventricular organs; COX2, cyclooxygenase-2; DAPI, 4′,6-diamidino-2-phenylindole dihydrochloride; FITC, fluorescein isothiocyanate isomer-I; GFP, green fluorescent protein; i.c.v., intracerebroventricular; Iba1, ionized calcium binding adapter molecule 1; LPS, lipopolysaccharide; LPS-RS, LPS from the photosynthetic bacterium *Rhodobacter sphaeroides*; IκBα, inhibitor of κB; ME, median eminence; MnPO, median preoptic nucleus; MPA, medial preoptic area; MW, molecular weight; NF-κB, nuclear factor-κB; NSCs, neural stem cells; NGS, normal goat serum; OVLT, organum vasculosum of the lamina terminalis; PBS, phosphate-buffered saline; PBST, PBS containing 0.3% Triton X-100; PFA, paraformaldehyde; PGE2, prostaglandin E2; PV-1, plasmalemmal vesicle-1; SFO, subfornical organ; PVN, paraventricular nucleus; TNF, tumor necrosis factor; IL, interleukin; SOX2, sex determining region Y-box 2; STAT3, signal transducer and activator of transcription factor 3; Sol, nucleus of the solitary tract; TLR, Toll-like receptor; VIPER, viral inhibitor peptide of TLR4; ZI, zona incerta

* Corresponding author at: Department of Applied Biology, Kyoto Institute of Technology, Kyoto 606-8585, Japan.
E-mail address: smiyata@kit.ac.jp (S. Miyata).

https://doi.org/10.1016/j.jneuroim.2018.04.017
Received 25 October 2017; Received in revised form 23 April 2018; Accepted 30 April 2018

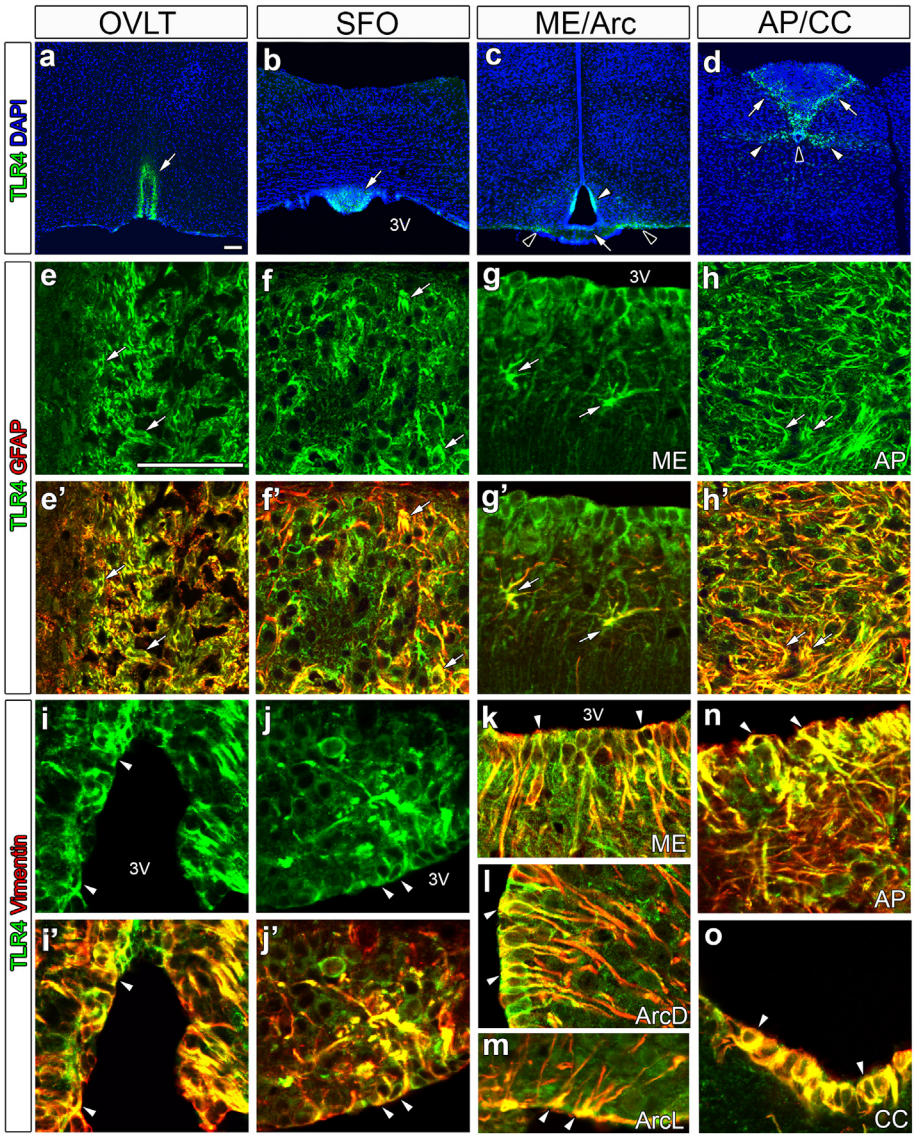

Fig. 1. High expression of TLR4 in astrocyte/tanycyte- like NSCs in the CVOs and Arc of adult mouse brains. a-d: Low magnification views showing many TLR4-expressing cells (arrows) in the CVOs such as the OVLT, SFO, ME, and AP (a-d). They were also observed in the dorsal (open arrowheads) and lateral parts (filled arrowheads) in the Arc (c), the commissural part of the Sol (open arrowheads), and CC (filled arrowheads) (d). e-h, e′-h′: Double-labeling immunohistochemistry revealed TLR4 expression in GFAP$^+$ astrocyte-like NSCs (arrows) in the OVLT (e, e′), SFO (f, f′), and AP (h, h′), and in GFAP$^+$ astrocytes in the ME (g, g′). i-o: TLR4 was highly expressed in vimentin$^+$ tanycyte-like NSCs (arrowheads) in the OVLT, SFO, ME, dorsal and lateral parts of the Arc, AP, and CC. 3 V, 3rd ventricle; ArcD, dorsal part of the Arc; ArcL, lateral part of the Arc. Scale bars = 50 μm.

cells in the hypothalamus, but it is independent of global PGE2 synthesis in the brain (Eskilsson et al., 2017).

The circumventricular organs (CVOs) are specialized brain regions that lack the normal blood-brain barrier (BBB) (Morita and Miyata, 2012) and initiate the early phase of brain neuroinflammatory responses. The expression of *Tlr4* mRNA is extremely high in the CVOs, including the organum vasculosum of the lamina terminalis (OVLT), subfornical organ (SFO), and area postrema (AP) (Laflamme and Rivest, 2001; Chakravarty and Herkenham, 2005). Moreover, our recent study revealed that TLR4 protein is expressed by neural stem cells (NSCs) in the CVOs of adult mouse (Nakano et al., 2015). NSCs were reported in the CVOs (Furube et al., 2015) and dorsal part of the Arc (Robins et al., 2013). Circulating LPS and/or cytokines cause faster transcriptional activation of genes encoding a wide variety of proinflammatory molecules in the CVOs compared with in other brain regions (Quan et al., 1997; Rummel et al., 2004, 2005, 2006; Sisó et al., 2010). Intraperitoneal and intracerebroventricular (i.c.v.) administration of LPS activates inflammatory signaling for nuclear translocation of the signal transducer and activator of transcription factor 3 (STAT3) in NSCs of CVOs (Rummel et al., 2004, 2005, 2006; Nakano et al., 2015; Yoshida et al., 2016). Furthermore, i.c.v. LPS increases TNF-α, IL-1β, and IL-6 levels in the mouse brain, and induces sickness behaviors, including reduced locomotor activity, social exploration, food intake (Park et al., 2011), and hyperthermia (Al-Saffar et al., 2013). Thus, TLR4 is highly expressed in the CVOs, but the functional significance of TLR4 in these regions for inflammatory signaling and thermoregulatory responses remains controversial, and direct in vivo studies are lacking.

Therefore, in this study, we examined the role of brain TLR4 in controlling signaling pathways and body temperature during LPS-induced inflammation and normal conditions using adult mice. First, we found that TLR4 was strongly expressed by astrocyte/tanycyte-like NSCs in the CVOs, Arc, and central canal (CC). Second, intraperitoneal administration of LPS induced NF-κB activation in astrocyte/tanycyte-like NSCs in the CVOs and dorsal part of the Arc, but caused NF-κB activation in only a few microglia. Intraperitoneal administration of LPS also activated NF-κB in endothelial cells throughout the brain. Third, the intracerebroventricular (i.c.v.) preadministration of low-dose TLR4 antagonists augmented LPS-induced hyperthermia, as well as inhibited NF-κB activation in astrocyte/tanycyte-like NSCs in the CVOs and dorsal part of the Arc. Lastly, i.c.v. high-dose TLR4 antagonists induced Fos expression not only in astrocyte/tanycyte-like NSCs in the CVOs and dorsal part of the Arc in normal mice, but also in neurons in thermoregulatory brain regions. Thus, the present study suggests that TLR4 on astrocyte/tanycyte-like NSCs in the CVOs and Arc acts as a central regulator to prevent excessive hyperthermia via NF-κB and Fos signaling during LPS-induced inflammatory conditions, in addition to

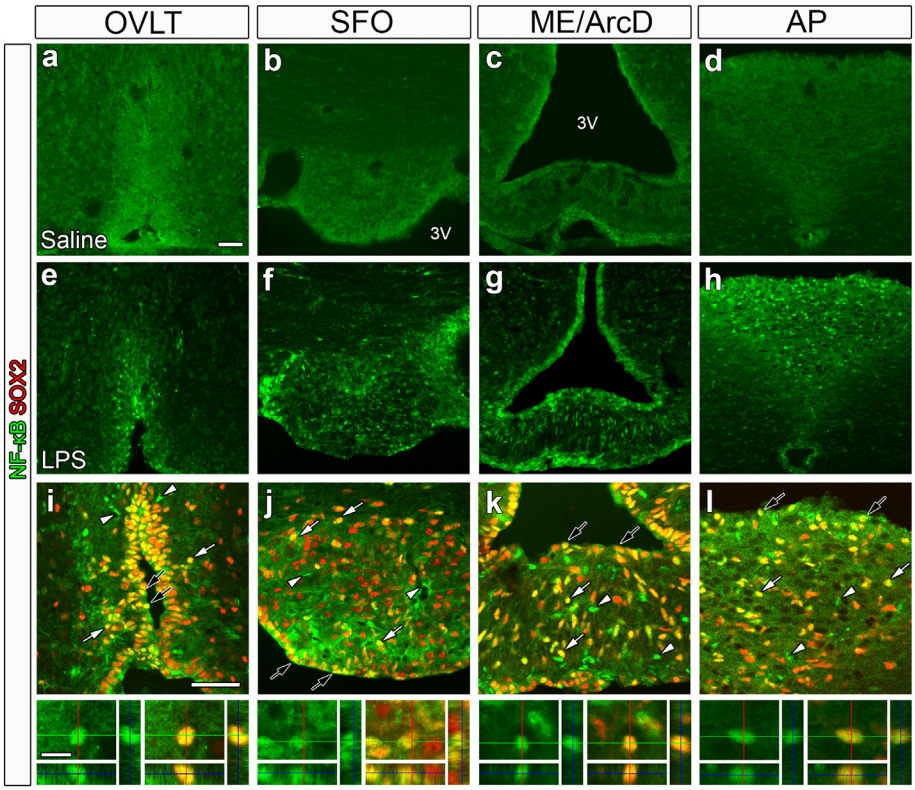

Fig. 2. Activation of NF-κB in astrocyte/tanycyte-like NSCs and astrocytes/tanycytes in the CVOs and dorsal part of the Arc in the adult mouse brain by systemic LPS stimulation. Mice received 50 μg/kg of LPS intraperitoneally and were sacrificed for NF-κB immunohistochemistry 2 h after the LPS stimulation. a-h: The nuclear translocation or activation of NF-κB was often observed in the CVOs and dorsal part of the Arc 2 h after systemic LPS stimulation, whereas NF-κB$^+$ nuclei were rarely seen in saline-treated controls. i-l: Double-labeling immunohistochemistry showing NF-κB$^+$ nuclei in SOX2$^+$ astrocyte-like NSCs in the OVLT, SFO, and AP, and in SOX2$^+$ astrocytes in the ME (open arrows). NF-κB$^+$ nuclei were also found in SOX2$^+$ tanycytes-like NSCs in the OVLT, SFO, and ME, and in SOX2$^+$ tanycytes in the AP (filled arrows). Three-dimensional image analysis demonstrated NF-κB$^+$ nuclei in SOX2$^+$ astrocyte-like NSCs (bottom panels in i-l). There was a significant number of NF-κB$^+$ SOX2-negative cells (open arrowheads) in the CVOs and Arc of LPS-treated animals. 3 V, 3rd ventricle; ArcD, dorsal part of the Arc. Scale bars = 10 (bottom panel in i), 50 (a and upper panel in i) μm.

maintaining a proper body temperature during normal conditions.

2. Methods

2.1. Animals

Adult male ICR mice (70–105 days old; Japan SLC Inc., Hamamatsu, Japan) were housed in a colony room under a 12-h light/dark cycle, and given ad libitum access to commercial chow and tap water. All experiments were performed in accordance with the guidelines of the NIH and Proper Conduct of Animal Experiments Science Council of Japan. The experimental protocol was approved by the Animal Ethics Experimental Committee of the Kyoto Institute of Technology.

2.2. Administration of LPS and TLR4 inhibitors

LPS from the photosynthetic bacterium *Rhodobacter sphaeroides* (LPS-RS ultrapure; Catalog # tlrl-prslps, molecular weight (MW) 2296.31) was purchased from InvivoGen (San Diego, CA). Viral inhibitor peptide of TLR4 (VIPER: KYSFKLILAEYRRRRRRRRR, purity 99.6%, MW 2780.31) was synthesized by GenScript (Piscataway, NJ). Stock solutions of LPS (1 mg/ml; Sigma-Aldrich, 055: type B5), LPS-RS ultrapure (2 mg/ml), and VIPER (10 mg/ml) were dissolved in pyrogen-free physiological saline (Otsuka Pharmaceutical Co. LTD.), stored at −80 °C, and diluted with pyrogen-free physiological saline prior to use. For i.c.v. administration, a stainless steel cannula (25-gauge) was implanted in each mouse under anesthesia with isoflurane with the tip laid in the lateral cerebral ventricle (0.3 mm anteroposterior and 1.0 mm lateral to the bregma, and 2.5 mm dorsoventral below the skull) using a standard stereotaxic technique (Paxinos and Franklin, 2001). Freely moving mice received i.c.v. administration (3 μl, 0.5 μl/min) of LPS-RS ultrapure (2 mg/ml, 200 μg/kg; 10 mg/ml, 1 mg/kg), VIPER (3 mg/ml, 300 μg/kg; 10 mg/ml, 1 mg/kg), or pyrogen-free physiological saline using a Model EP-1000E administration pump (Melquest, Toyama, Japan). For Fos immunohistochemistry, animals were sacrificed 2 h after administration of LPS-RS ultrapure or VIPER. For systemic LPS stimulation, mice received a single intraperitoneal dose of LPS in pyrogen-free physiological saline (5 μg/ml, 0.3 ml; 50 μg/kg) with or without the i.c.v. preadministration of TLR4 inhibitors, and were fixed for immunohistochemistry 2 h after LPS stimulation.

2.3. Immunohistochemistry

After deep anesthesia with isoflurane, mice were perfused intracardially with PBS (pH 7.4) containing 5 U/ml heparin followed by 4% paraformaldehyde (PFA) in 0.1 M phosphate buffer (PB; pH 7.4). Fixed brains were cryoprotected using 30% sucrose in phosphate-buffered saline (PBS; pH 7.4) and frozen quickly in Tissue-Tek OCT compound (Sakura Finetechnical, Tokyo, Japan). Sections were obtained in a coronal cut by cryostat (Leica, Wetzlar, Germany) at a thickness of 30 μm. For immunofluorescence staining, the standard technique described in our previous study was performed on free-floating sections (Furube et al., 2015, 2018). In brief, sections were washed with PBS and treated with 25 mM glycine in PBS for 20 min to quench the remaining fixative aldehyde. Sections were preincubated with 5% normal goat serum (NGS) in PBS containing 0.3% Triton X-100 (PBST) at 4 °C for 24 h and then incubated with the primary antibody in PBST containing 1% NGS at 4 °C for 72 h. The following primary antibodies were used: guinea pig polyclonal antibody against laminin (the antigen was laminin-111 from Engellbreth-Holm-Swarm murine sarcoma basement membrane: IM-2011; dilution 1:200, Imamura et al., 2010) and glial fibrillar acidic protein (GFAP; YN-GFAP2012-Pig; dilution 1:400, Nakano et al., 2015); goat polyclonal antibody against sex determining region Y-box 2 (SOX2; sc-17,320, SantaCruz; dilution 1:2000); rabbit polyclonal antibody against Fos (sc-52, Santa Cruz; dilution 1:3000), nuclear factor-κ B 65 (NF-κB p65; sc-372, Santa Cruz; dilution 1:1000), TLR4 (SPC-200, StressMarq, dilution 1:200), and ionized calcium binding adapter molecule 1 (Iba1; 019-19741, WAKO; dilution 1:800); rat monoclonal antibody against CD11b (5C6, BIO-RAD, dilution 1:10,000) and plasmalemmal vesicle-1 (PV-1; MECA32, HSHB; dilution 1:20); chicken polyclonal antibody against vimentin (AB5733, Chemicon; dilution 1:12,000). After several washes with PBST, they were

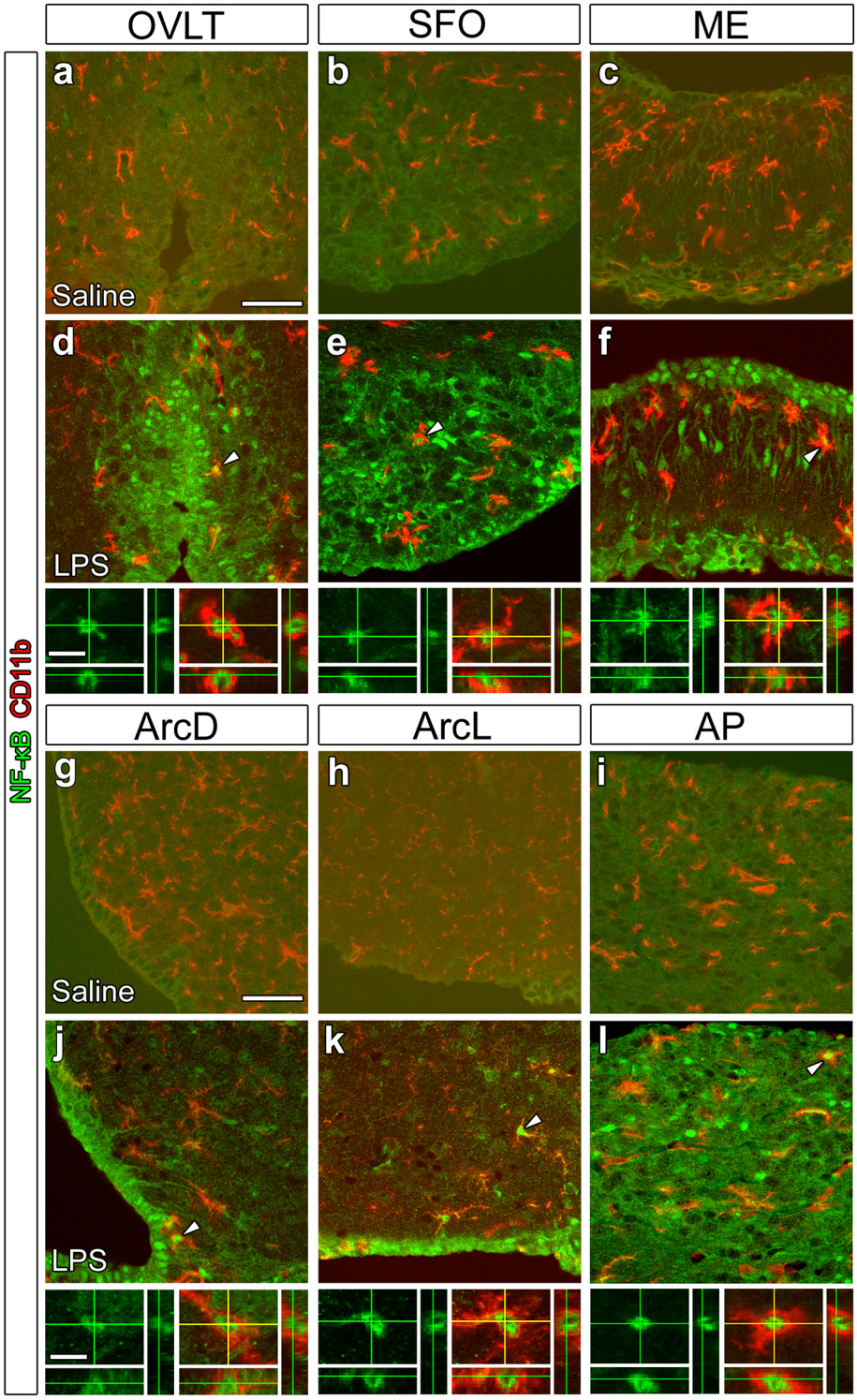

Fig. 3. Activation of NF-κB in microglia in the CVOs and neighboring regions in adult mouse brains by systemic LPS stimulation. Mice received 50 μg/kg of LPS intraperitoneally and were sacrificed for NF-κB immunohistochemistry 2 h after LPS stimulation. a-c, g-i: Nuclear translocation or activation of NF-κB was rarely seen in microglia in saline-treated control animals. d-f, j-l: NF-κB$^+$ nuclei were observed in a few CD11b$^+$ microglia (open arrowheads). ArcD, dorsal part of the Arc. ArcL, lateral part of the Arc. Scale bars = 10 (bottom panel in d and j), 50 (a and g) μm.

further incubated with an Alexa 405-, 488-, or 594-conjugated secondary goat antibody (Jackson ImmunoResearch, dilution 1:400). To confirm the specificity of the TLR4 antibody, TLR4 (SPC-200, Stress-Marq) was preincubated with a synthetic immunogen peptide corresponding to amino acids 420–435 of human TLR4 (GLEQLEHLDFQH-SNLK, GenScript). For nuclear staining, sections were incubated with 4′,6-diamidino-2-phenylindole dihydrochloride solution (DAPI; Dojindo, Kumamoto, Japan; dilution 1:1000).

For visualization of endothelial cells, we transcardially perfused fluorescein isothiocyanate isomer-I (FITC; catalog # F007, Dojindo, Kumamoto, Japan; MW 389.38) according to our previously reported method (Miyata and Morita, 2011; Miyata, 2015; Miyata, 2017). Briefly, after anesthesia with isoflurane, mice received the following transcardiac perfusions; first, oxygenated PBS (pH 7.0) containing 5 U/

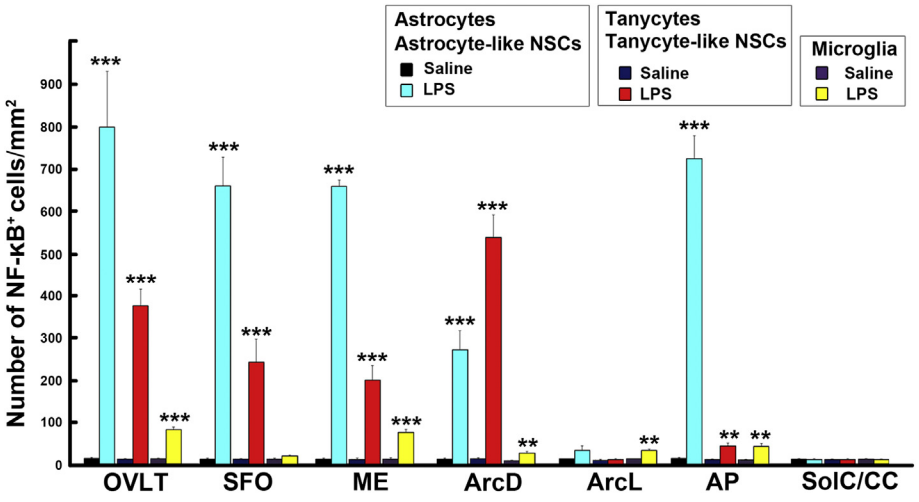

Fig. 4. Quantitative analysis demonstrating activation of NF-κB in astrocytes/astrocyte-like NSCs, tanycytes/tanycyte-like NSCs, and microglia in the CVOs and their neighboring regions in adult mouse brains by systemic LPS stimulation. Mice received 50 μg/kg of LPS intraperitoneally and were sacrificed for NF-κB immunohistochemistry 2 h after LPS stimulation. The number of NF-κB$^+$ nuclei in SOX2$^+$ astrocytes/tanycyte-like NSCs, tanycytes/tanycyte-like NSCs, and microglia was increased in the CVOs and neighboring brain regions following systemic LPS stimulation. ArcD, dorsal part of the Arc; ArcL, lateral part of the Arc; SolC, commissural part of the Sol. Data (n = 4) were expressed as the mean (± s.e.m.). **: P < 0.01, ***: P < 0.001 between the saline control and LPS by the unpaired Student's *t*-test.

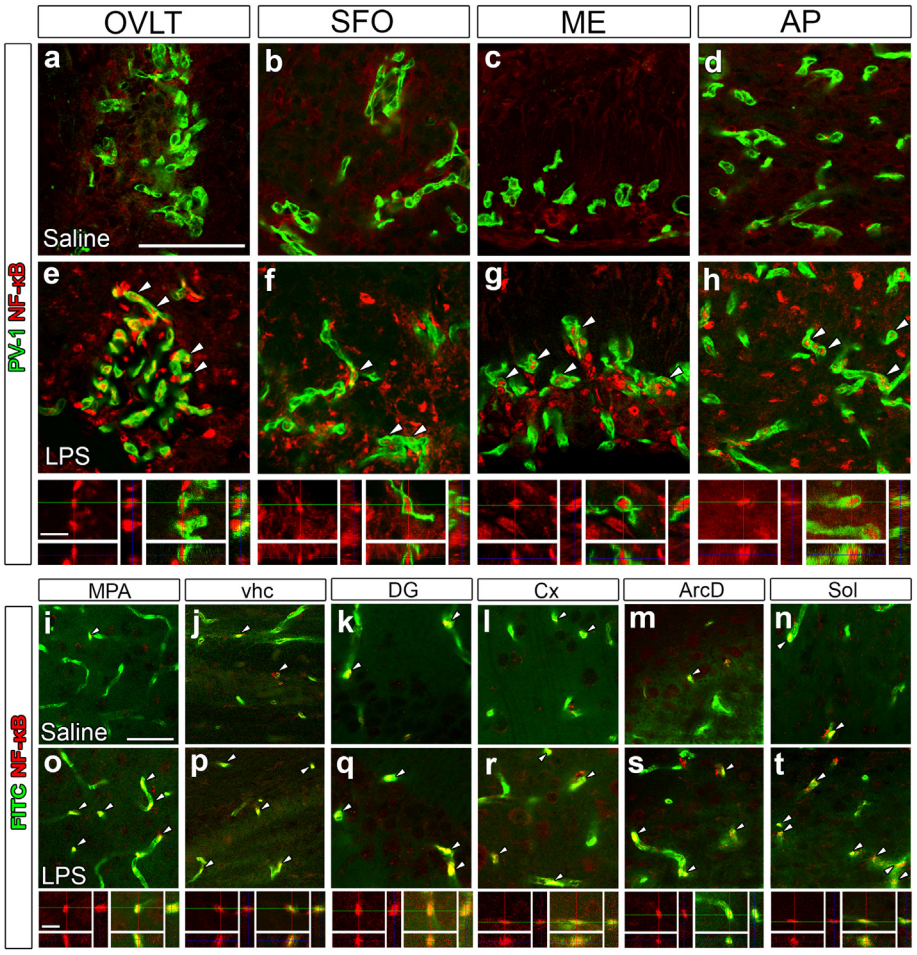

Fig. 5. NF-κB activation in endothelial cells in the adult mouse brain by systemic LPS stimulation. Mice received 50 μg/kg of LPS intraperitoneally and were then sacrificed for NF-κB immunohistochemistry 2 h later. a-h: NF-κB$^+$ nuclei (arrowheads) were often observed in PV-1$^+$ endothelial cells in the CVOs after systemic LPS stimulation (e-h), whereas they were rarely seen in saline-treated controls (a-d). Three-dimensional image analysis demonstrated NF-κB$^+$ nuclei in endothelial cells (bottom panels in e-h). i-t: NF-κB$^+$ nuclei (arrowheads) were often observed in FITC-incorporated endothelial cells in the medial preoptic area, ventral hippocampal commissure, dentate gyrus, cerebral cortex, dorsal part of the Arc, and Sol after LPS stimulation. vhc, ventral hippocampal commissure; DG, dentate gyrus; Cx, cerebral cortex; ArcD, dorsal part of the Arc; ArcL, lateral part of the Arc. Scale bars = 10 (bottom panel in e and o), 50 (a, i) μm.

ml of heparin and 10 mM glucose for 1 min; second, FITC (0.1 mg/ml) in oxygenated PBS (pH 7.0) for 5 min; third, oxygenated PBS (pH 7.0) for 1 min; finally, 4% PFA in 0.1 M PB (pH 8.0) for 10 min at 4 °C. After the transcadiac perfusion of the fixative, brains were dissected, post-fixed in 4% PFA in 0.1 M PB (pH 8.0) at 4 °C overnight, and then placed in 30% sucrose in PBS (pH 8.0) at 4 °C for 24 h. The preparation of frozen sections and immunohistochemical procedure were performed as described above.

2.4. Confocal observation and quantification

For confocal microscopic observations, coverslips were sealed with Vectashield (Vector Labs, Burlingame, CA) and observed using a laser-scanning confocal microscope (LSM-510, Carl Zeiss or TCS SP2 Leica). We selected at least 5 sections per animal from the OVLT and 7 sections per animal from the other brain regions according to the mouse brain atlas (Paxinos and Franklin, 2001). For quantitative analysis, confocal images were obtained under the same pinhole size, brightness, and contrast settings. In the case of NF-κB, we set the threshold for contrast

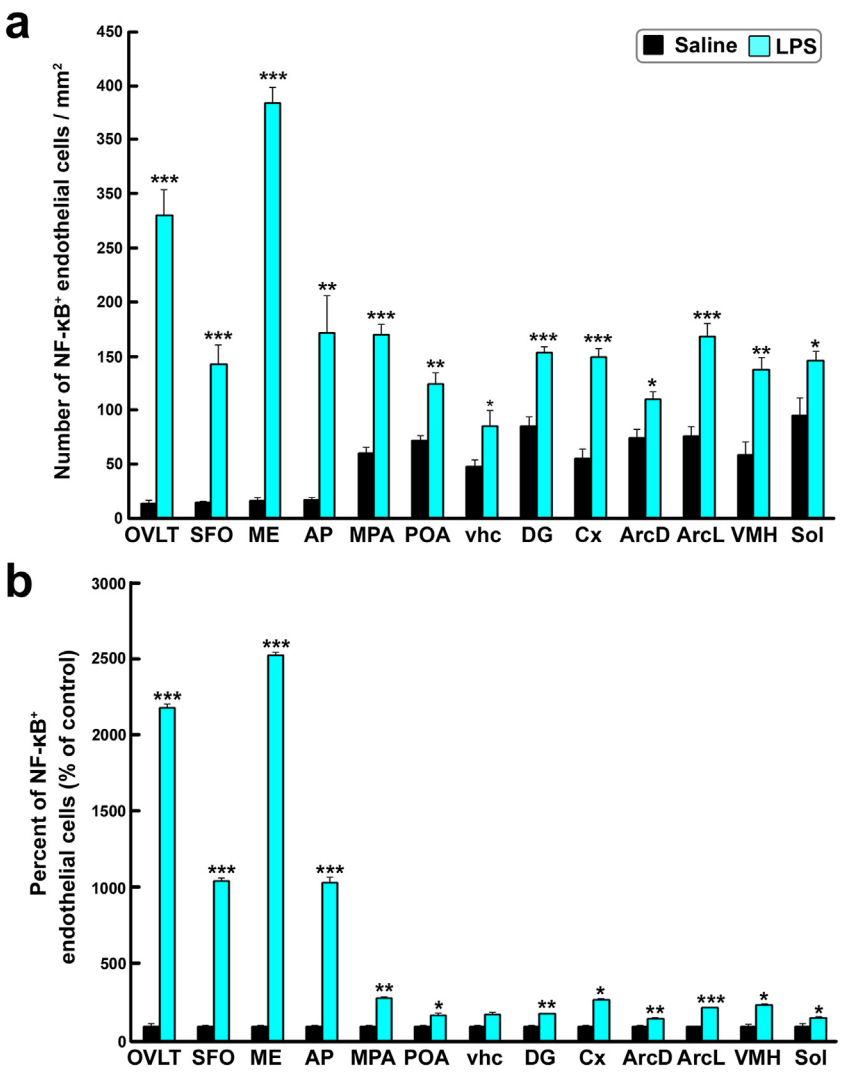

Fig. 6. Quantitative analysis showing NF-κB activation in endothelial cells in the adult mouse brain by systemic LPS stimulation. Mice received 50 μg/kg of LPS intraperitoneally and were then sacrificed for NF-κB immunohistochemistry 2 h later. a: Quantitative analysis demonstrated that the density of NF-κB$^+$ endothelial cells in all examined brain regions was significantly increased by systemic LPS stimulation. The density of NF-κB$^+$ endothelial cells in saline-treated controls was lower in the CVOs than that in other brain regions. b: The percentage of NF-κB$^+$ endothelial cells was also significantly increased in most examined brain regions by systemic LPS stimulation. vhc, ventral hippocampal commissure; DG, dentate gyrus; Cx, cerebral cortex; ArcD, dorsal part of the Arc; ArcL, lateral part of the Arc; VMH, ventromedial hypothalamus. Data (n = 4) were expressed as the mean (± s.e.m.). *: P < 0.05, **: P < 0.01, ***: P < 0.001 between the saline control and LPS by the unpaired Student's *t*-test.

on confocal microscopy to preferentially detect strong signals in the nucleus. We saved images (1024 × 1024 pixels) as TIFF files using the Zeiss LSM image browser or TCS SP2 AOBS, and arranged them using Photoshop CC (Adobe, San Jose, CA). On quantitative analyses, the total area of each brain region was measured using WinRoof, an image analyzing system (Mitani Corporation, Fukui, Japan). The numbers of Fos- and NF-κB-positive nuclei in SOX2-labeled astrocytes and ependymal cells, and PV-1-positive or FITC-incorporated endothelial cells were counted using WinRoof, for which the threshold intensity was set to include measurement profiles by visual inspection and held constant. The experimenter was blinded to the treatment group for analysis of all images. Differences were assessed using a significance level of $P < 0.05$ with the unpaired Student's *t*-test or ANOVA with Tukey post-hoc test.

2.5. Measurement of body temperature

Mice were anesthetized with chloral hydrate and a transponder (G2 E-mitter) that recorded core body temperature was implanted intraperitoneally two weeks after implantation of a stainless canula. They were then housed at an ambient temperature of 25 °C under a 12-h light/dark cycle (lights on at 7:00 A.M.) and monitored for at least 1 week after the implantation of the telemeter. LPS and TLR4 antagonists were administered between 11.00 h and 12.00 h. Mice received 50 μg/kg of LPS intraperitoneally 30 min after the i.c.v. administration of LPS-RS ultrapure (200 μg/kg), VIPER (300 μg/kg), or pyrogen-free saline, and were then sacrificed for NF-κB immunohistochemistry 2 h later. In some experiments, mice received the i.c.v. LPS-RS ultrapure (200 μg/kg or 1 mg/kg), VIPER (300 μg/kg or 1 mg/kg), or pyrogen-free saline, and were fixed for the immunohistochemistry 2 h later. Abdominal temperature was measured by biotelemetry at 5-min intervals, and plotted in 10-min intervals over a period of 2 h before and 6 h after the treatment. Data were acquired and evaluated using Vital View software (VitalView series 4000). The fever index (°C × hr) was calculated as the area under the temperature curve based on the mean temperature during a period of 2 h before the intraperitoneal administration.

3. Results

3.1. Expression of TLR4 in circumventricular NSCs

On low magnification, TLR4 expression was prominent in the CVOs: OVLT (Fig. 1a), SFO (Fig. 1b), ME (Fig. 1c), and AP (Fig. 1d). No specific fluorescent signal was detected when the primary antibody was preincubated with a synthetic immunogen peptide corresponding to amino acids 420–435 of TLR4 (Supplementary Fig. 1). TLR4-expressing cells were also noted in the dorsal and lateral parts of the Arc (Fig. 1c), commissural part of the solitary nucleus (Sol), and CC (Fig. 1d). GFAP-expressing cells in the OVLT, SFO, and AP expressed the NSC marker nestin and exhibited proliferative activity, consistent with our previous finding that GFAP-expressing cells are astrocyte-like NSCs (Furube

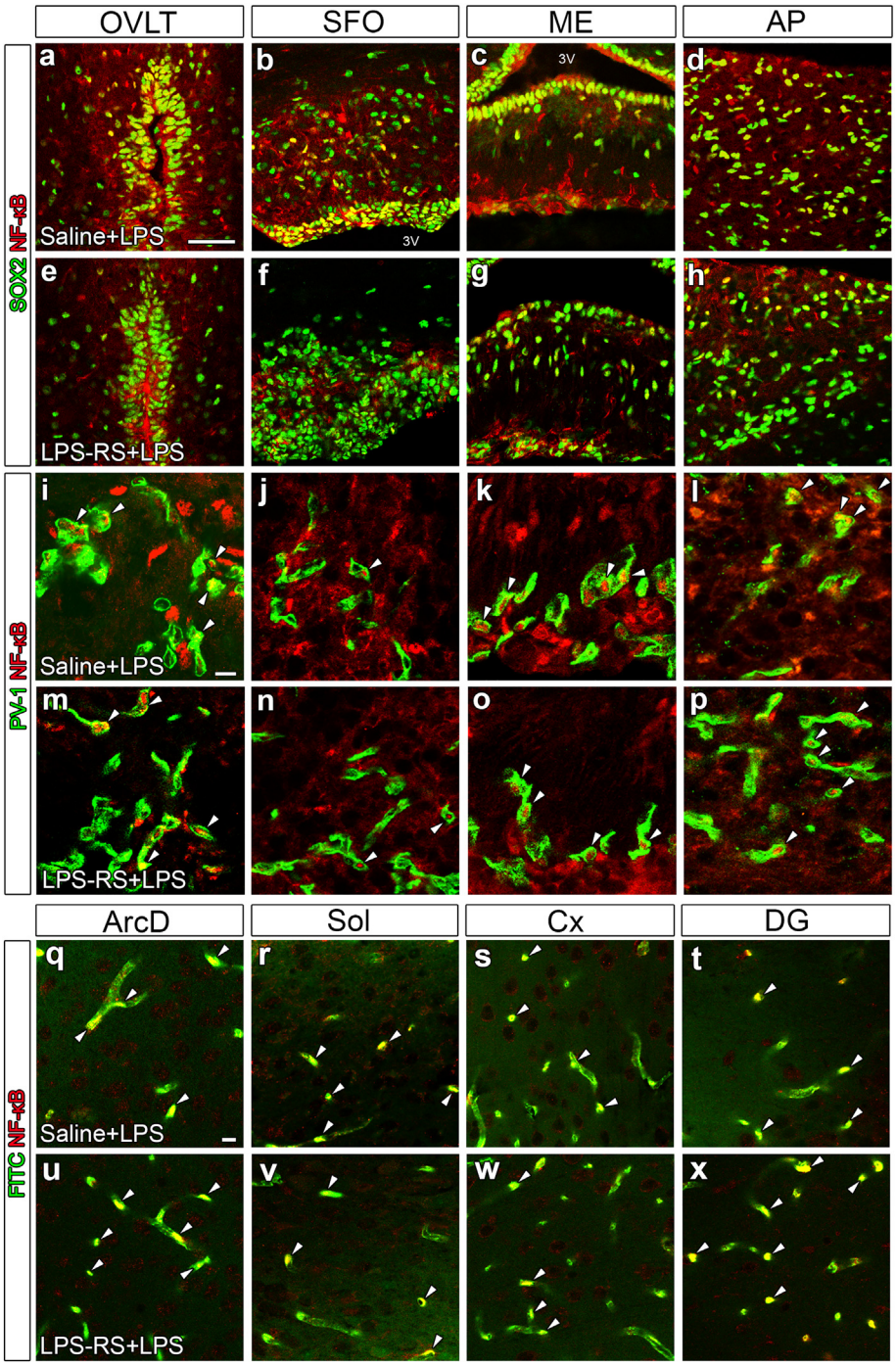

Fig. 7. Effects of the TLR4 inhibitor LPS-RS ultrapure on NF-κB activation in astrocytes/astrocyte-like NSCs, tanycyte/tanycyte-like NSCs, and endothelial cells in the adult mouse brain by systemic LPS stimulation. Mice received 50 μg/kg of LPS intraperitoneally 30 min after i.c.v. administration of the TLR4 inhibitor LPS-RS ultrapure (200 μg/kg), and were then sacrificed for NF-κB immunohistochemistry 2 h after LPS stimulation. a-h: NF-κB$^+$ nuclei were frequently observed in SOX2$^+$ astrocyte/astrocyte-like NSCs and tanycytes/tanycyte-like NSCs in the CVOs and dorsal part of the Arc of LPS-treated animals (a-d), but i.c.v. preadministration of LPS-RS ultrapure greatly decreased the number of NF-κB$^+$ nuclei in SOX2$^+$ cells in these regions (e-h). i-p: The i.c.v. preadministration of LPS-RS ultrapure did not alter the number of NF-κB$^+$ nuclei (arrowheads) in PV-1$^+$ endothelial cells in the CVOs. q-x: The i.c.v. preadministration of LPS-RS ultrapure did not alter the number of NF-κB$^+$ nuclei in FITC-incorporated endothelial cells. ArcD, dorsal part of the Arc; Cx, cerebral cortex; DG, dentate gyrus. Scale bars = 10 (i, q), 50 (a) μm.

et al., 2015). High magnification of double-labeled immunohistochemistry revealed TLR4 expression on cellular bodies and processes of GFAP$^+$ astrocyte-like NSCs in the OVLT (Fig. 1e, e′), SFO (Fig. 1f, f′), and AP (Fig. 1h, h′), and on those of GFAP$^+$ astrocytes in the ME (Fig. 1g, g′). Tanycytes in the CVOs and Arc are specialized ependymal cells located on the ventricle wall that have long cellular processes extending deep into brain parenchyma (Rodríguez et al., 2010; Langlet et al., 2013), and were reported to be NSCs (Lee et al., 2012; Robins et al., 2013; Furube et al., 2015). Double-labeled immunohistochemistry demonstrated LR4 expression on cellular bodies and processes of vimentin$^+$ tanycyte-like NSCs in the OVLT (Fig. 1i, i′), SFO (Fig. 1j, j′), ME (Fig. 1k), dorsal parts of the Arc (Fig. 1l), and CC (Fig. 1o), and on those of vimentin$^+$ ependymal cells in the lateral parts of the Arc (Fig. 1m) and AP (Fig. 1n). On the other hand, TLR4 immunoreactivity was below detectable limits on endothelial cells in the CVOs (Supplementary Fig. 2a-d) and other brain regions (Supplementary Fig. 2e-l). Taken together, these results indicate that TLR4 is highly expressed by circumventricular astrocyte/tanycyte-like NSCs.

3.2. NF-κB activation in NSCs and microglia by systemic LPS stimulation

We previously clarified the brain cells in which systemic LPS stimulation activates NF-κB in adult mice. Activated NF-κB dimers are translocated from the cytosol to the nucleus after dissociation from IκBα monomers (Ghosh et al., 1998; Perkins, 2007). As the p65 and p50 subunits are the most common in NF-κB dimers, nuclear translocation of the p65 subunit is useful to evaluate activation of NF-κB (Maguire et al., 2011). Thus, we used an antibody against the NF-κB p65 subunit

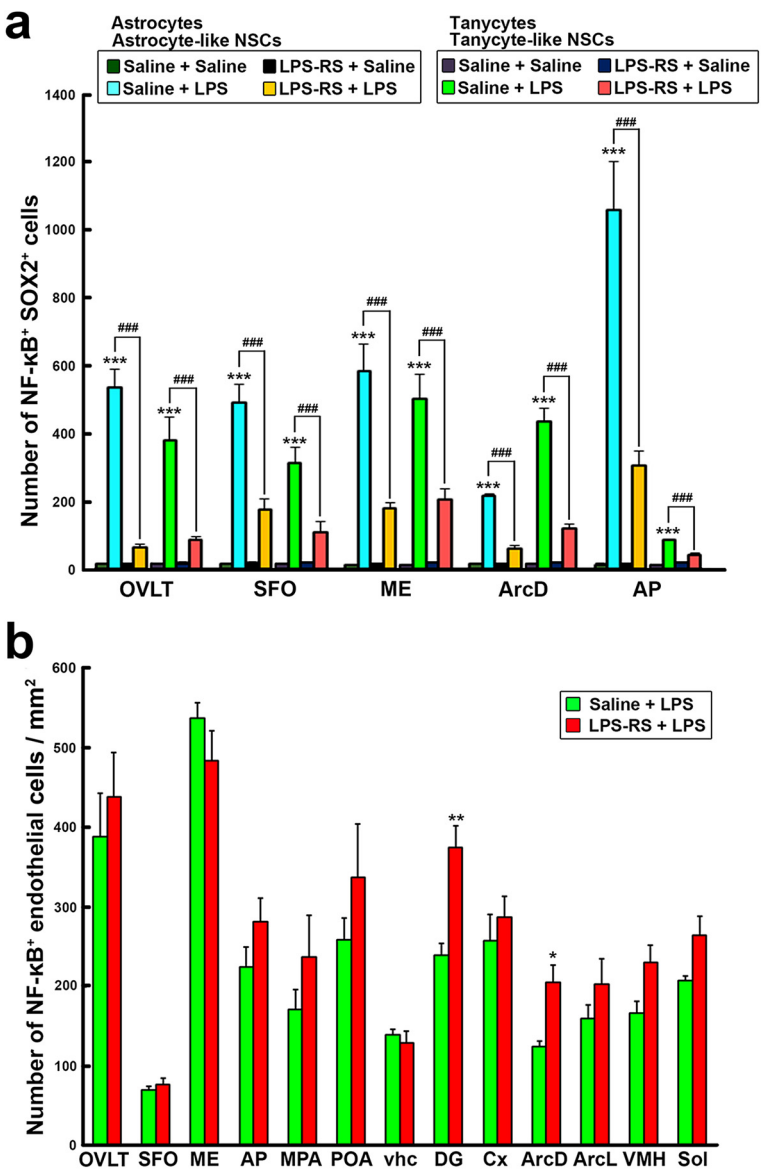

Fig. 8. Quantitative analysis of the effects of i.c.v. preadministration of the TLR4 inhibitor LPS-RS ultrapure on NF-κB activation in astrocytes/astrocyte-like NSCs, tanycyte/tanycyte-like NSCs, and endothelial cells in adult mice. Mice received 50 μg/kg of LPS intraperitoneally 30 min after the i.c.v. administration of the TLR4 inhibitor LPS-RS ultrapure (200 μg/kg), and were then sacrificed for NF-κB immunohistochemistry 2 h after LPS stimulation. a: The i.c.v. preadministration of LPS-RS ultrapure significantly decreased the number of NF-κB$^+$ astrocytes/astrocyte-like NSCs and tanycyte/tanycyte-like NSCs in the CVOs and dorsal part of the Arc. b: The i.c.v. preadministration of LPS-RS ultrapure did not significantly alter the number of NF-κB$^+$ endothelial cells in the CVOs or other brain regions, except in the dentate gyrus and dorsal part of the Arc. ArcD, dorsal part of the Arc. Data (n = 4) were expressed as the mean (± s.e.m.). ***: $P < 0.001$ between the saline + saline and saline + LPS, ###: $P < 0.001$ between saline + LPS and LPS-RS ultrapure + LPS by ANOVA with Tukey's post hoc test.

to assess activation of NF-κB by immunohistochemistry. On low magnification, intraperitoneal administration of 50 μg/kg of LPS induced nuclear translocation and activation of NF-κB in the OVLT (Fig. 2e), SFO (Fig. 2f), ME, Arc (Fig. 2g), and AP (Fig. 2h), but NF-κB activation was absent in saline-treated control mice (Fig. 2a-d). Double-labeled immunohistochemistry revealed NF-κB$^+$ nuclei in SOX2$^+$ astrocyte-like NSCs in the OVLT (Fig. 2i), SFO (Fig. 2j), AP (Fig. 2l), and dorsal part of the Arc (Supplementary Fig. 3a-a″) and in SOX2$^+$ astrocytes in the ME (Fig. 2k), but not in SOX2$^+$ astrocytes in the commissural part of the Sol (Supplementary Fig. 3b-b″) or lateral part of the Arc (Supplementary Fig. 3c-c″). Three- dimensional remodeling of confocal images confirmed the presence of NF-κB$^+$ nuclei within SOX2$^+$ astrocyte-like NSCs in the OVLT, SFO, and AP, and within SOX2$^+$ astrocytes in the ME (Fig. 2i-l). NF-κB activation was also observed in SOX2$^+$ tanycyte-like NSCs in the OVLT (Fig. 2i), SFO (Fig. 2j), ME (Fig. 2k), dorsal part of the Arc (Supplementary Fig. 3a-a″), and in SOX2$^+$ ependymal cells in the AP (Fig. 2l), but not in the CC (Supplementary Fig. 3b-b″) or lateral part of the Arc (Supplementary Fig. 3c-c″). Double-labeling immunohistochemistry with a microglia marker demonstrated NF-κB$^+$ nuclei in a few CD11b$^+$ microglia in the CVOs and their neighboring brain regions (Fig. 3).

On quantitative analysis, the number of NF-κB$^+$ SOX2$^+$ astrocyte-like NSCs in the CVOs and dorsal part of the Arc was significantly increased by systemic LPS stimulation (Fig. 4). The number of NF-κB$^+$ SOX2$^+$ tanycyte-like NSCs in the CVOs and dorsal part of the Arc was also significantly increased by systemic LPS stimulation. In contrast, systemic LPS stimulation did not significantly increase the number of NF-κB$^+$ SOX2$^+$ astrocytes or tanycytes in the lateral part of the Arc and commissural part of the Sol, or that of SOX2$^+$ tanycyte-like NSCs in the CC. Collectively, these results indicate that systemic LPS induces NF-κB activation in astrocyte/tanycyte-like NSCs in the CVOs and dorsal part of the Arc.

3.3. NF-κB signaling in endothelial cells by systemic LPS stimulation

We next examined whether NF-κB activation occurs in endothelial cells in the brain after systemic LPS stimulation because NF-κB$^+$ nuclei were also observed in SOX2-negative cells in LPS-treated animals (Fig. 2i-l and Supplementary Fig. 3a″-c″). IL-1β was reported to induce NF-κB activation and PGE2 synthesis in brain endothelial cells as well as elicit hyperthermia (Ching et al., 2007; Eskilsson et al., 2014). Intraperitoneal administration of 50 μg/kg of LPS increased the number of NF-κB$^+$ endothelial cells in the OVLT (Fig. 5e), SFO (Fig. 5f), ME (Fig. 5g), and AP (Fig. 5h) on double-labeling immunohistochemistry

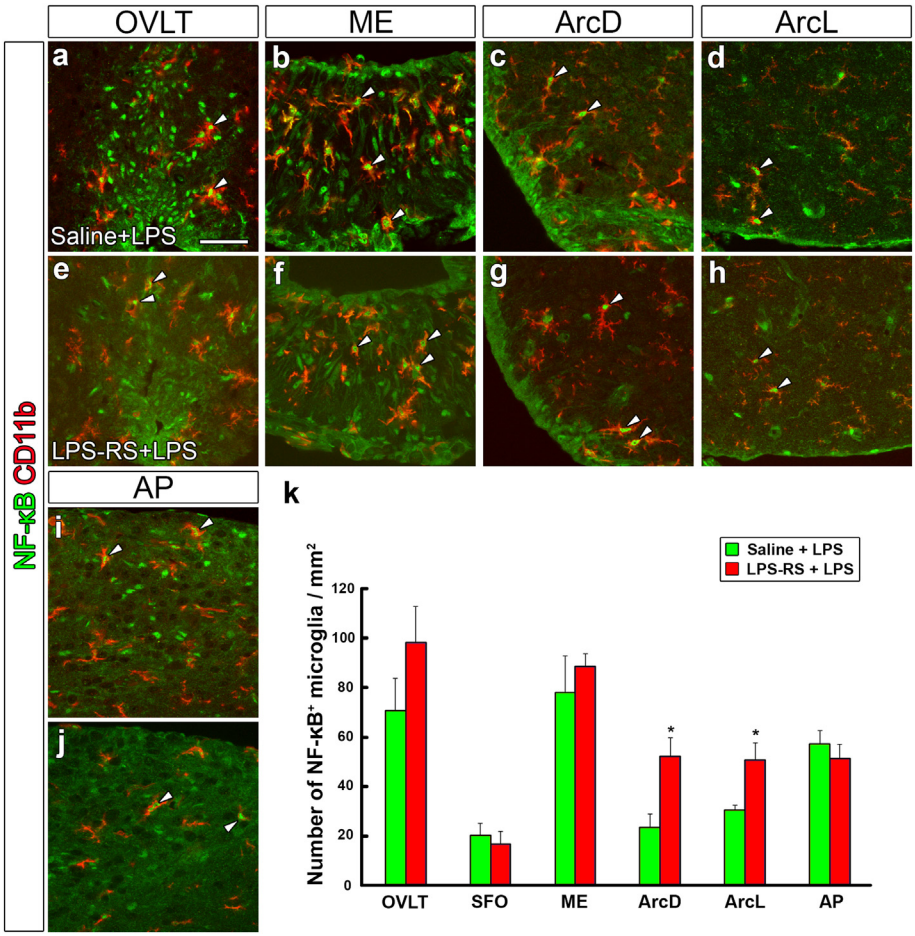

Fig. 9. Effects of the i.c.v. preadministration of LPS-RS ultrapure on the number of NF-κB$^+$ nuclei in microglia in the adult mouse brain. Mice received 50 μg/kg of LPS intraperitoneally 30 min after i.c.v. administration of the TLR4 inhibitor LPS-RS ultrapure (200 μg/kg), and were then sacrificed for NF-κB immunohistochemistry 2 h after LPS stimulation. a-j: The i.c.v. preadministration of LPS-RS ultrapure did not decrease the number of NF-κB$^+$ nuclei in CD11b-positive microglia. Scale bars = 50 μm. k: The i.c.v. preadministration of LPS-RS ultrapure did not significantly alter the number of NF-κB$^+$ microglia in the OVLT, SFO, ME, or AP, but it significantly increased the number of NF-κB$^+$ microglia in the dorsal and lateral part of the Arc. ArcD, dorsal part of the Arc; ArcL, lateral part of the Arc. Data (n = 4) were expressed as the mean (± s.e.m.). *: $P < 0.05$ between the saline + LPS and LPS-RS ultrapure + LPS by the unpaired Student's *t*-test.

with the endothelial cell marker PV-1, whereas NF-κB$^+$ endothelial cells were rarely seen in saline-treated control mice (Fig. 5a-d). In our previous study, endothelial cells were able to incorporate FITC into their nuclei (Miyata and Morita, 2011). Moreover, systemic LPS also increased the number of NF-κB$^+$ nuclei in FITC-incorporated endothelial cells in other brain regions, such as the medial preoptic area (MPA), ventromedial hippocampal commissure (vhc), dentate gyrus, cerebral cortex, the dorsal part of the Arc, and Sol (Fig. 5o-t), compared with in saline-treated controls (Fig. 5i-n). Three-dimensional remodeling of confocal images confirmed the presence of NF-κB$^+$ nuclei within endothelial cells (Fig. 5e-h, 5o-t).

By quantitative analysis, the number of NF-κB$^+$ endothelial cells was found to be significantly increased in the OVLT, SFO, ME, and AP by the intraperitoneal administration of 50 μg/kg of LPS (Fig. 6a). In other brains regions, the number of NF-κB$^+$ endothelial cells was also significantly increased. The density of NF-κB$^+$ endothelial cells was relatively lower in the CVOs (< 35 cells/mm^2) compared with that in other brain regions (> 50 cells/mm^2) of saline-treated control animals (Fig. 6a). Therefore, the percent increase of NF-κB$^+$ endothelial cells was higher in the CVOs than that in other brain regions (Fig. 6b).

3.4. Effects of a low-dose TLR4 inhibitor, LPS-RS ultrapure, on NF-κB activation by LPS-induced inflammation

We next investigated whether TLR4 is responsible for LPS-induced NF-κB activation in astrocyte/tanycyte-like NSCs in the CVOs. We used a specific TLR4 inhibitor, LPS-RS ultrapure, which is known to bind with myeloid differentiation factor 2, thereby inhibiting the interaction of TLR4 with LPS or endogenous TLR4 ligands (Coats et al., 2005). The i.c.v. preadministration of LPS-RS ultrapure at a dose of 200 μg/kg greatly attenuated NF-κB activation in SOX2$^+$ astrocyte/tanycyte-like NSCs and astrocytes/tanycytes in the CVOs (Fig. 7e-h) compared with that by saline-LPS treatment (Fig. 7a-d). However, the i.c.v. preadministration of LPS-RS ultrapure had no effect on LPS-induced NF-κB activation in endothelial cells in the CVOs (Fig. 7i-p) or other brain regions (Fig. 7q-x).

The quantitative analysis demonstrated that pretreatment with LPS-RS ultrapure significantly attenuated the LPS-induced increase in NF-κB$^+$ nuclei in SOX2$^+$ astrocyte/tanycyte-like NSCs or astrocytes/tanycytes in the CVOs and dorsal part of the Arc (Fig. 8a). However, pretreatment with LPS-RS ultrapure did not significantly affect the LPS-induced increase in the number of NF-κB$^+$ nuclei in endothelial cells of LPS-stimulated mice compared with that in saline-LPS-treated mice (Fig. 8b). There was one exception in which LPS-RS ultrapure promoted the LPS-induced increase in the number of NF-κB$^+$ nuclei in endothelial cells in the dentate gyrus and dorsal part of Arc. Pretreatment with LPS-RS ultrapure did not significantly alter the LPS-induced increase in the number of NF-κB$^+$ nuclei in microglia in LPS-stimulated mice compared with that in saline control mice (Fig. 9). These results suggest that LPS-induced NF-κB activation in astrocyte/tanycyte-like NSCs in the CVOs and dorsal part of the Arc is mediated via TLR4.

3.5. A low dose of TLR4 inhibitors augments LPS-induced hyperthermia by activating Fos in the CVOs and Arc

Hyperthermia is a hallmark of bacterial infection and an important host defense response. Therefore, we investigated whether TLR4 in the brain regulates body temperature under inflammatory conditions. We used two specific TLR4 inhibitors, LPS-RS ultrapure and VIPER. VIPER contains a cell-penetrating delivery sequence and inhibits TLR4

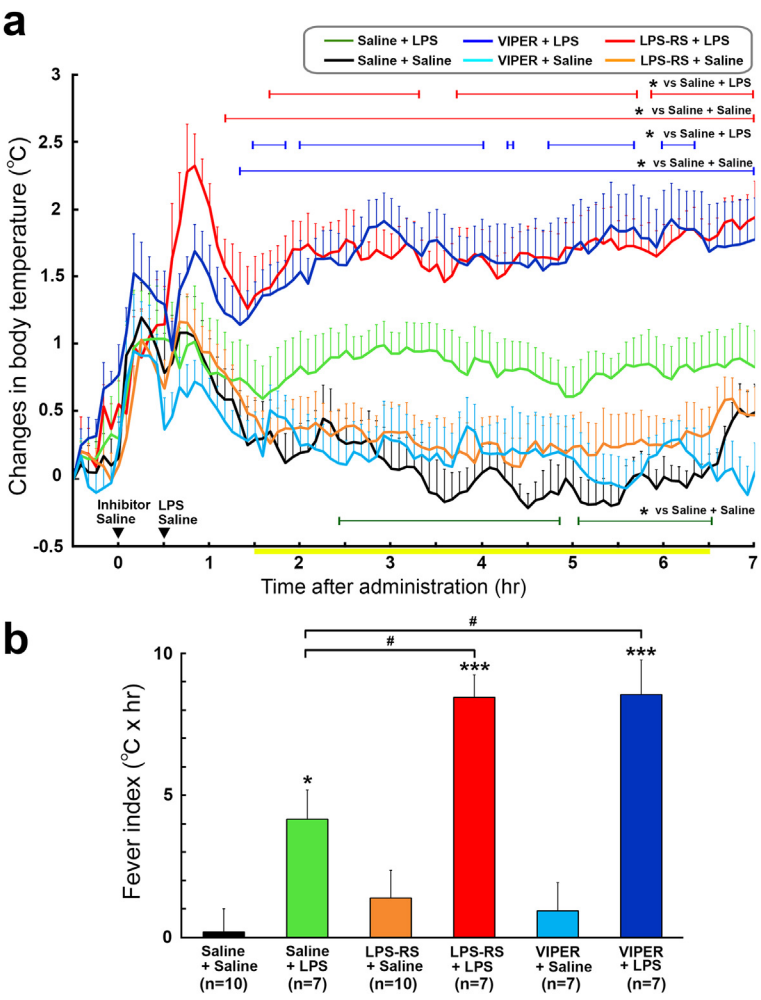

Fig. 10. Effects of the i.c.v. preadministration of low-dose TLR4 inhibitors, LPS-RS ultrapure and VIPER, on abdominal core temperatures under normal and LPS-induced inflammatory conditions. Mice received 50 μg/kg of LPS intraperitoneally 30 min after i.c.v. administration of a TLR4 inhibitor, LPS-RS ultrapure (200 μg/kg) or VIPER (300 μg/kg), and body temperature was measured with a G2 E-mitter transponder that was implanted intraperitoneally. a: Mice in all experimental groups initially exhibited a stress-induced increase in mean body temperature during/after the administration procedure. The intraperitoneal administration of LPS at 50 μg/kg significantly increased the mean body temperature. LPS-induced hyperthermia was augmented when 200 μg/kg of LPS-RS ultrapure was infused into the brain ventricle 30 min before the intraperitoneal administration of 50 μg/kg of LPS. The i.c.v. preadministration of 300 μg/kg of VIPER also promoted LPS-induced hyperthermia. Neither 200 μg/kg of LPS-RS ultrapure nor 300 μg/kg of VIPER directly affected the mean body temperature. The yellow line indicates the measured period for the fever index. b: The fever index of saline-LPS-treated animals was significantly higher than that of saline-saline-treated controls. The i.c.v. preadministration of the TLR4 inhibitors significantly increased the fever index in mice with LPS-induced hyperthermia compared with that in saline-LPS-treated mice, but these inhibitors did not significantly alter the fever index. *: $P < 0.05$ between two groups by unpaired Student's t-test (a) and *: $P < 0.05$, ***: $P < 0.001$ vs Saline + saline, #: $P < 0.05$ vs Saline + LPS by ANOVA with Tukey's post hoc test (b). (For interpretation of the references to colour in this figure legend, the reader is referred to the web version of this article.)

signaling by interacting with intracellular TLR4 adaptor proteins (Lysakova-Devine et al., 2010). We measured the core body temperature in response to pharmacological treatments in mice fitted with a G2 E-mitter, which allows for free movement, and access to water and food. All mice initially exhibited stress-induced transient hyperthermia on handling during/after the administration procedure regardless of whether LPS or saline was given (Fig. 10a and Supplemantary Table 1). Intraperitoneal administration of 50 μg/kg of LPS increased body temperatures at 145–290 and 305–395 min, with a peak (0.99 ± 0.18 °C) at 175 min. The i.c.v. administration of either 200 μg/kg of LPS-RS ultrapure or 300 μg/kg of VIPER was performed 30 min before the intraperitoneal administration of 50 μg/kg of LPS. The i.c.v. preadministration of 200 μg/kg of LPS-RS ultrapure significantly promoted LPS-induced hyperthermia at 95–200, 225–345, and 355–420 min, with a peak (1.90 ± 0.27 °C) at 420 min. Similarly, the i.c.v. preadministration of 300 μg/kg of VIPER significantly increased LPS-induced hyperthermia at 90–110, 120–250, 260, 285–340, and 360–380 min, with a peak (1.86 ± 0.28 °C) at 365 min. Although administration of 200 μg/kg of LPS-RS ultrapure or 300 μg/kg of VIPER alone did not significantly change the body temperature, intraperitoneal administration of 50 μg/kg of LPS significantly increased the fever index compared with in the saline-saline-treated control (Fig. 10b). Taken together, these results indicate that low-dose TLR4 inhibitors promote LPS-induced hyperthermia without induction of hyperthermia by the inhibitor itself.

To clarify if the TLR4 inhibitors LPS-RS ultrapure and VIPER acted on TLR4-expressing astrocyte/tanycyte-like NSCs in the CVOs, we performed Fos immunohistochemistry using the animals that received i.c.v. administration of the TLR4 inhibitor. On low magnification, Fos^+ nuclei were seen in the OVLT (Fig. 11a), SFO (Fig. 11b), and ME (Fig. 11c), but not in the AP (Fig. 11d). Double-labeling immunohistochemistry demonstrated that the i.c.v. administration of 200 μg/kg of LPS-RS ultrapure increased the number of Fos^+ nuclei in $SOX2^+$ astrocyte/tanycyte-like NSCs, and astrocytes/tanycytes in the OVLT (Fig. 11i), SFO (Fig. 11j), ME (Fig. 11k), CC (Fig. 11m), and Arc (Fig. 11l,n), but not in the AP (Supplementary Fig. 4a, b), whereas Fos^+ nuclei were rarely observed in saline-treated control mice (Fig. 11e-h). On quantitative analysis, pretreatment with LPS-RS ultrapure significantly reduced the number of Fos^+ nuclei in $SOX2^+$ astrocyte/tanycyte-like NSCs in the CVOs and Arc (Fig. 11o). Similarly, the i.c.v. administration of 300 μg/kg of VIPER increased the number of Fos^+ nuclei in $SOX2^+$ astrocyte/tanycyte-like NSCs, and astrocytes/tanycytes in the OVLT, SFO, ME, Arc, and CC, but not in the AP (Fig. 12 and Supplementary Fig. 4a, c). These results suggest that i.c.v. administration of low-dose TLR4 inhibitors induces Fos activation in astrocyte/tanycyte-like NSCs mainly in the CVOs and in astrocytes in thermoregulation-associated hypothalamic regions.

3.6. *High doses of TLR4 inhibitors cause hyperthermia and Fos activation in normal animals*

We then investigated whether TLR4 functions as a negative regulator for brain thermogenic pathways in normal animals. As the i.c.v. administration of 200 μg/kg of LPS-RS ultrapure or 300 μg/kg of VIPER did not siginificantly affect the body temeperature (Fig. 10), high doses of TLR4 inhibitors, such as 1 mg/kg of LPS-RS ultrapure or 1 mg/kg of

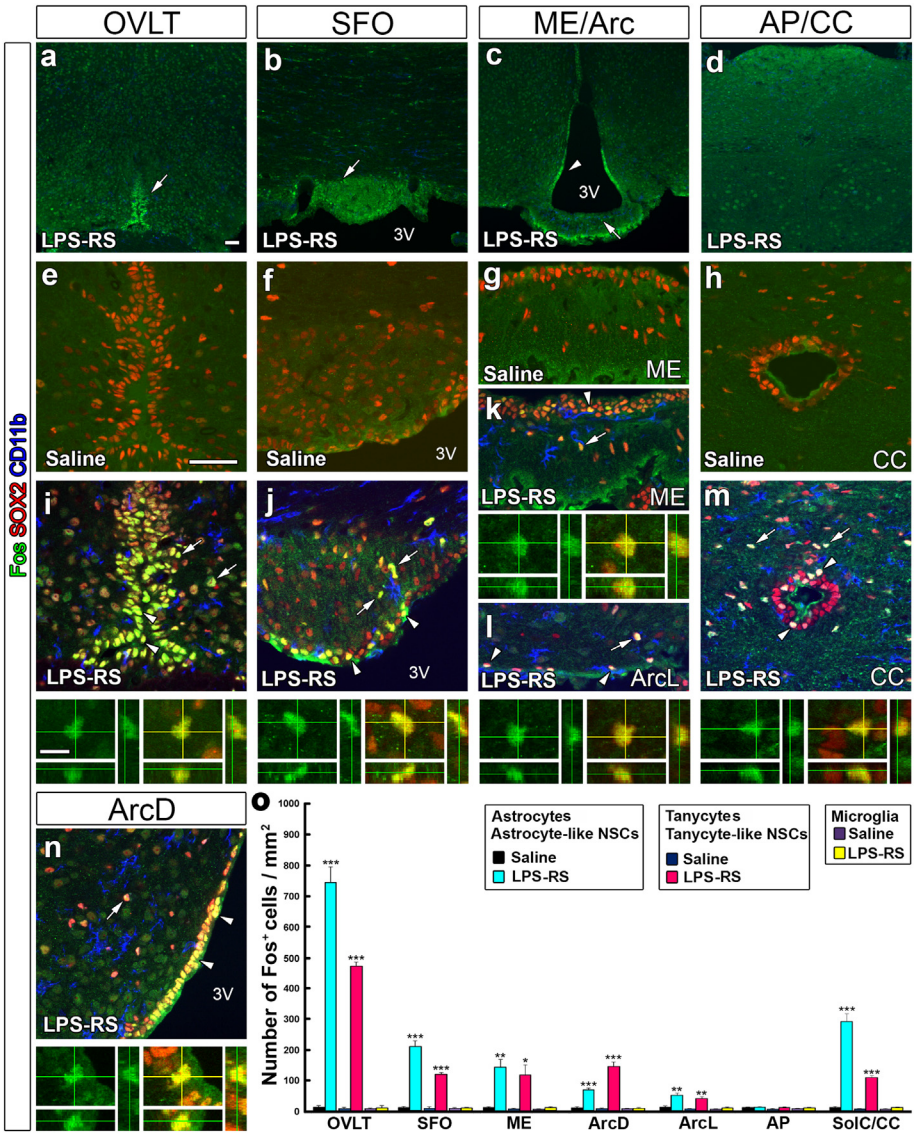

Fig. 11. Effects of i.c.v. administration of a low-dose TLR4 inhibitor, LPS-RS ultrapure, on Fos expression in the CVOs and neighboring brain regions in normal adult mice. Mice received i.c.v. administration of 200 μg/kg of LPS-RS ultrapure and were sacrificed for Fos immunohistochemistry 2 h later. a-h: Many Fos^+ nuclei (arrows) were observed in the CVOs and neighboring brain regions, except in the AP, in LPS-RS ultrapure -infused animals, but almost no Fos^+ nuclei were found in the saline-treated controls. i-n: On high magnification, Fos^+ nuclei were frequently observed in $SOX2^+$ astrocytes/astrocyte-like NSCs (arrows) and tanycyte/tanycyte-like NSCs (arrowheads) in the CVOs and neighboring brain regions, whereas they were rare in $CD11b^+$ microglia (i-n). Scale bars = 10 (bottom panel in i) and 50 (a and e) μm. o: Based on the quantitative analysis, i.c.v. administration of LPS-RS ultrapure significantly increased the number of Fos^+ astrocytes/astrocyte-like NSCs and tanycyte/tanycyte-like NSCs but not microglia in the CVOs, Arc, and Sol. ArcD, dorsal part of the Arc; ArcL, lateral part of the Arc. Data (n = 4) were expressed as the mean (± s.e.m.). *: $P < 0.05$, **: $P < 0.01$, ***: $P < 0.001$ between the saline control and LPS-RS ultrapure by the unpaired Student's *t*-test.

VIPER, were given. Mice initially exhibited stress-induced transient hyperthermia by handling during/after i.c.v. administration regardless of whether a TLR4 inhibitor or saline was injected (Fig. 13a and Supplementary Table 2). The i.c.v. administration of 1 mg/kg of LPS-RS ultrapure significantly increased hyperthermia at 40–80 and 100–420 min, with a peak (1.59 ± 0.27 °C) at 225 min. Similarly, the i.c.v. administration of 1 mg/kg of VIPER significantly increased hyperthermia at 60 and 125–420 min, with a peak (2.05 ± 0.22 °C) at 405 min. Furthermore, i.c.v. administration of both 1 mg/kg of LPS-RS ultrapure and 1 mg/kg of VIPER significantly increased the fever index compared with that in the saline-injected controls (Fig. 13b).

To clarify the TLR4-associated thermogenic pathway in the brain, we examined TLR4 inhibitor-dependent activation of brain glial and neuronal cells by Fos immunohistochemistry. With high-dose LPS-RS ultrapure (1 mg/kg), Fos^+ nuclei were observed in $SOX2^+$ astrocyte/tanycyte-like NSCs in the OVLT (Fig. 14a, e) and SFO (Fig. 14d, h), and in $SOX2^+$ astrocytes in the ME (Fig. 14l, q). Although there were few Fos^+ nuclei in HuC/D^+ neurons in the OVLT and SFO (Fig. 14e′, h′), some were observed in HuC/D^+ neurons in the ME (Fig. 14q). Almost no Fos^+ nuclei were found in the AP, as was observed with low-dose LPS-RS ultrapure (data not shown). In addition to the CVOs, the administration of high-dose LPS-RS ultrapure induced Fos activation in both $SOX2^+$ astrocytes and HuC/D^+ neurons in the MPA (Fig. 14c, g, g′), paraventricular nucleus (PVN; Fig. 14j, n, n′), and arcuate nucleus (Arc; Fig. 14l, p). In the median preoptic nucleus (MnPO; Fig. 14b, f, f′), zona incerta (ZI; Fig. 14i, m, m′), and anterior hypothalamic area (AH; Fig. 14k, o, o′), however, Fos^+ nuclei were mainly observed in HuC/D^+ neurons rather than in $SOX2^+$ astrocytes. Animals that received i.c.v. high-dose (1 mg/kg) VIPER were similar (Fig. 15).

4. Discussion

It is well-known that TLR4 plays an important role in inflammatory responses and hyperthermia, particularly in the initial peripheral interaction between the infection of Gram-negative bacteria and macrophages/dendritic cells. However, data regarding the role of brain TLR4 in inflammatory responses is limited. The present study suggests that TLR4 in astrocyte/tanycyte-like NSCs in the circumventricular brain regions acts as a central controller to prevent excessive hyperthermia in LPS-induced inflammatory conditions, in addition to maintaining a proper body temperature under normal conditions. Furthermore, we found that TLR4 in the CVOs functions opposite peripheral TLR4, underlying the unique features of the CVOs and astrocyte- and tanycyte-like NSCs within.

Previous in situ hybridization studies reported that *Tlr4* mRNA was highly expressed in the CVOs (Laflamme and Rivest, 2001; Chakravarty

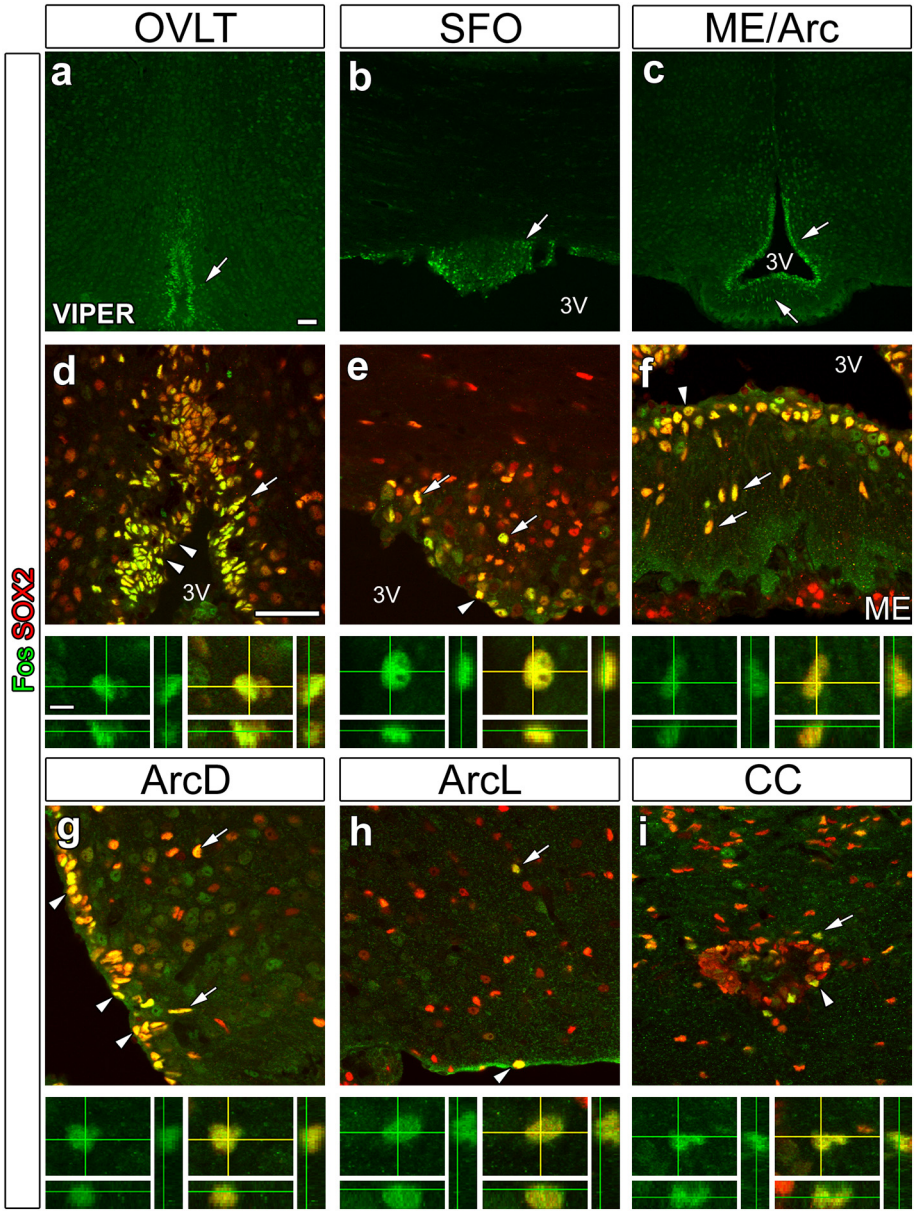

Fig. 12. Effects of the i.c.v. administration of a low-dose TLR4 inhibitor, VIPER, on Fos expression in the CVOs and neighboring brain regions in normal adult mice. Mice received i.c.v. administration of 300 μg/kg of VIPER and were sacrificed for Fos immunohistochemistry 2 h later. a-c: Many Fos^+ nuclei (arrows) were observed in the CVOs and Arc of VIPER-infused animals. d-i: On high magnification, Fos^+ nuclei were frequently observed in $SOX2^+$ astrocytes/astrocyte-like NSCs (arrows) and tanycyte/tanycyte-like NSCs (arrowheads) in the CVOs and Arc. ArcD, dorsal part of the Arc; ArcL, lateral part of the Arc. Scale bars = 50 μm.

and Herkenham, 2005). Moreover, our previous immunohistochemical study demonstrated that TLR4 was expressed in astrocyte-like NSCs in the OVLT, SFO, and AP (Nakano et al., 2015). Moreover, a previous report found a marked increase in IκBα mRNA expression in CVOs in LPS-inflamed animals (Quan et al., 1997; Chakravarty and Herkenham, 2005). The present study further revealed that TLR4 was strongly expressed in tanycyte-like NSCs in the CVOs, Arc, and CC, and peripheral administration of LPS significantly induced NF-κB activation in these cells. LPS is a hydrophilic molecule, and is therefore unable to pass through the relatively impermeable BBB to directly activate relevant thermoregulatory parenchyma cells in the brain. It was recently proposed that LPS is incorporated into brain parenchyma via a lipoprotein-mediated transport mechanism in the CVOs (Vargas-Caraveo et al., 2017). Taken together, these results demonstrate that TLR4 is expressed in astrocyte/tanycyte-like NSCs in the CVOs and Arc, and systemic LPS stimulation induces NF-κB signaling in astrocyte/tanycyte-like NSCs instead of in microglia in the circumventricular brain regions.

The early phase of LPS-induced hyperthermia (< 2 h after LPS stimulation) was previously reported to be triggered by TLR4 signaling in hematopoietic cells (Romanovsky et al., 2006; Steiner et al., 2006). In contrast, the late phase of LPS-induced hyperthermia (2–6 h after LPS stimulation) may depend on TLR4-dependent activation of central and peripheral hematopoietic cells, and nonhematopoietic cells, such as endothelial cells, microglia, and astrocytes, in the brain (Romanovsky et al., 2006; Steiner et al., 2006). The systemic administration of low-dose LPS (50–100 μg/kg) induces hyperthermia, whereas that of high-dose LPS (> 1 mg/kg) causes hypothermia (Oka et al., 2003). In the present study, pretreatment with low-dose TLR4 inhibitors increased the magnitude of the late phase of LPS-induced hyperthermia and sustained its duration along with attenuation of NF-kB signaling in circumventricular astrocyte/tanycyte-like NSCs. Peripheral TLR4 is essential for LPS-induced hyperthermia (Steiner et al., 2006). The intravenous administration of E5564, an analog of LPS-RS, almost completely inhibited LPS-induced production of blood cytokines in vivo and

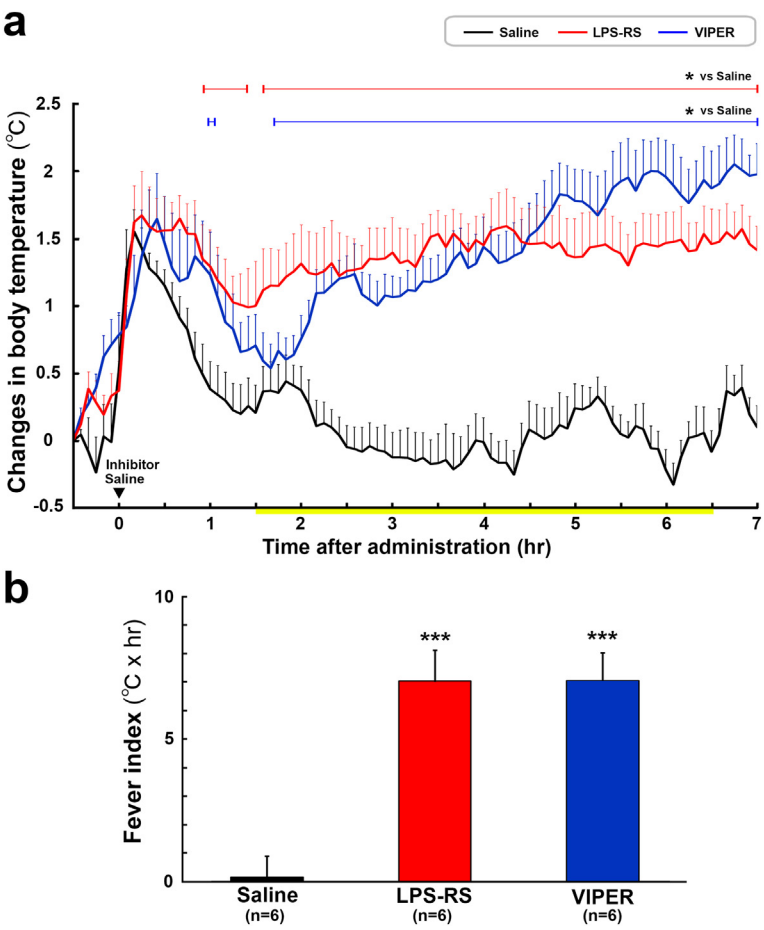

Fig. 13. Effects of i.c.v. administration of high-dose TLR4 inhibitors, LPS-RS ultrapure and VIPER, on abdominal core temperatures under normal conditions. Mice received i.c.v. administration of a TLR4 inhibitor, LPS-RS ultrapure (1 mg/kg) or VIPER (1 mg/kg), and body temperature was measured with a G2 E-mitter transponder that was implanted intraperitoneally. a: Animals in all experimental groups initially exhibited stress-induced elevation of body temperature during/after the administration procedure. The i.c.v. administration of LPS-RS ultrapure induced marked continuous hyperthermia. The i.c.v. administration VIPER also markedly increased the mean body temperature. The yellow line indicates the period of the measured fever index. b: The i.c.v. administration of both LPS-RS ultrapure and VIPER significantly increased the fever index compared with that in saline-treated control mice. *P < 0.05 between two groups by the unpaired Student's *t*-test (a) and ***: P < 0.001 vs Saline by ANOVA with Tukey post hoc test (b). (For interpretation of the references to colour in this figure legend, the reader is referred to the web version of this article.)

in vitro, as well as reduced LPS-induced mortality (Mullarkey et al., 2003). The i.c.v. administration of LPS at a dose of 0.2–2 μg/kg induced hyperthermia, possibly via the activation of endothelial cells (Al-Saffar et al., 2013; Cao et al., 1999). It was suggested that brain uptake of circulating LPS was so minimal that most effects of peripherally administered LPS are likely mediated by TLR4 located outside the BBB (Banks and Robinson, 2010; Murray et al., 2011). Substances less than MW 3000 have high vascular permeability in the CVOs, whereas those greater than MW 10,000 are impermeable, suggesting the MW size limit to be < 10,000 (Morita and Miyata, 2012; Morita et al., 2016). Although LPS is heterogeneous and tends to form aggregates of varying sizes, negating the meaning of MW, it is estimated to be in the range of 1–4 million or greater (Jann et al., 1975). Recently, however, it was reported that LPS was detected in parenchyma in the CVOs (Vargas-Caraveo et al., 2017). Thus, LPS may diffuse into parenchyma and directly stimulate TLR4 in the CVOs, leading to the notable difference in function of brain TLR4 from peripheral TLR4.

Alternative mechanisms for TLR4 activation in the CVOs include the participation of endogenous TLR4 ligands because many proteins have been identified as endogenous TLR4 ligands (Yu et al., 2014). High-mobility group box 1 was reported to be released in response to LPS or IFN-α stimulation without necrotic cell death (Lu et al., 2014). In the present study, the i.c.v. administration of low-dose TLR4 antagonists significantly induced Fos expression specifically in astrocyte/tanycyte-like NSCs in the OVLT, SFO, and Arc, and in astrocytes in the ME. The administration of low-dose TLR4 antagonists induced Fos expression in TLR4-expressing cells in these regions, and Fos expression was rare in neurons. Moreover, the present study demonstrated that high-dose TLR4 antagonists significantly elevate body temperature and induce neuronal Fos expression in thermoregulation-associated hypothalamic regions, such as the MPA and MnPO, in normal animals. The MPA, MnPO, and AH in the hypothalamus are known as the main thermoregulatory centers that drive sympathetic nerve activity to control heat production (Lazarus et al., 2007; Nakamura, 2011; Contreras et al., 2016; Eskilsson et al., 2017). Stimulation of the Arc neurons increased sympathetic nerve activity and thermogenesis of brown adipose tissue via activation of neurons in the hypothalamic PVN and dorsomedial nuclei (Chitravanshi et al., 2016). The ZI receives input from hypothalamic nuclei, the locus coeruleus, raphe complex, parabrachial area, and medial districts of the pontomedullary reticular formation (Shammah-Lagnado et al., 1985). The ZI is also known to function in thermoregulation because direct stimulation of the ZI alters the baseline temperature of brown fat tissue (Kelly and Bielajew, 1996.). Thus, it is possible that TLR4 on astrocyte/tanycyte-like NSCs in circumventricular brain regions is continuously activated in order to control thermogenic pathways of the brain to suppress excessive hyperthermia during LPS-induced inflammation, in addition to maintaining the body temperature under normal conditions.

In the present study, LPS-induced activation of NF-kB signaling was observed in endothelial cells in all examined brain regions. On the other hand, intraperitoneal administration of LPS induced NF-κB activation in only a few microglia in the CVOs. Moreover, pretreatment with the TLR4 antagonist augmented LPS-induced hyperthermia without affecting NF-kB activation in endothelial cells. Although no visible TLR4 immunoreactivity in endothelial cells was detected on immunohistochemistry, in situ hybridization study revealed the expression of *Tlr4* mRNA in endothelial cells (Chakravarty and Herkenham, 2005). In the present study, i.c.v. preadministration of low-dose TLR4 antagonists attenuated NF-kB activation in astrocyte/tanycyte-like NSCs in circumventricular brain regions, but did not affect NF-kB activation in endothelial cells. As antagonists in the ventricular CSF may have limited access to endothelial cells, the proinflammatory cytokines

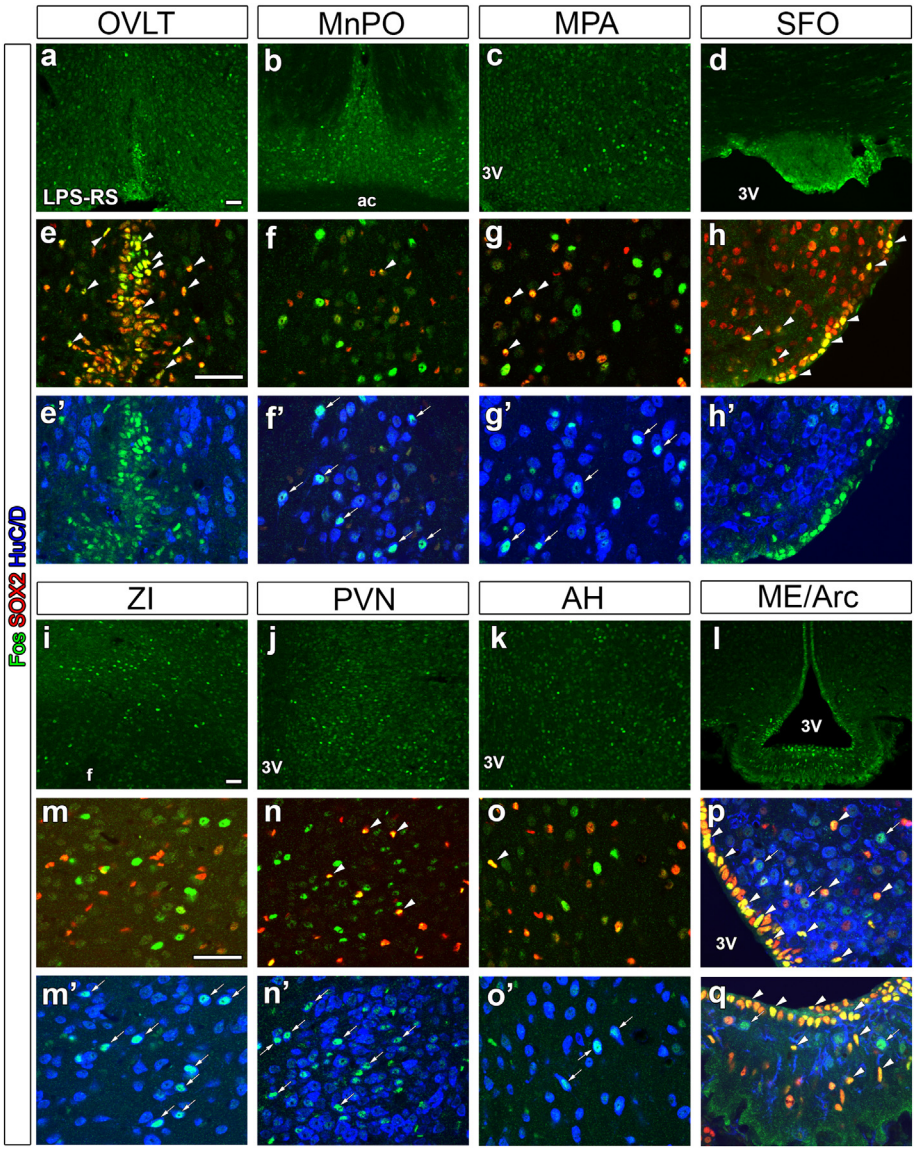

Fig. 14. Effects of i.c.v. administration of a high-dose TLR4 inhibitor, LPS-RS ultrapure, on Fos expression in normal adult mice. Mice received i.c.v. administration of 1 mg/kg of LPS-RS ultrapure and were sacrificed for Fos immunohistochemistry 2 h later. a-d, i-l: On low magnification, many Fos$^+$ nuclei were observed in the MnPO, MPA, ZI, PVN, AH, and Arc, similarly the CVOs such as the OVLT, SFO, and ME. e-h, e′-h′, m-q, m′-o′: In the CVOs and dorsal part of the Arc, many Fos$^+$ nuclei were observed in SOX2$^+$ astrocyte/tanycyte-like NSCs (arrowheads) in the OVLT (e), SFO (h), and Arc (p), and in SOX2$^+$ astrocytes in the ME (q) and dorsal part of the Arc (p). Fos$^+$ nuclei were not found in HuC/D$^+$ neurons (arrows) in the OVLT (e′) or SFO (h′), but they were detected in the Arc (p) and ME (q). In other brain regions, Fos$^+$ nuclei were frequently observed in SOX2$^+$ astrocytes (arrowheads) and HuC/D$^+$ neurons (arrows) in the MnPO (f, f′), MPA (g, g′), and PVN (n, n′). On the other hand, Fos$^+$ nuclei were more frequent in HuC/D$^+$ neurons (arrows) than in SOX2$^+$ astrocytes (arrowheads) in the ZI (m, m′) and AH (o, o′). Scale bars = 50 μm.

TNF-α and IL-1β may be able to activate NF-κB and regulate target gene transcription (Hayden and Ghosh, 2004; Lawrence, 2009). Systemic LPS induced strong and rapid expression of *IκBα* mRNA in endothelial cells lining the BBB in large and small blood vessels (Quan et al., 1997; Laflamme et al., 1999). Furthermore, selective deletion of COX-2 in brain endothelial cells attenuates hyperthermia (Wilhelms et al., 2014; Nilsson et al., 2016). Recently, LPS-induced hyperthermia was reported to strongly correlate with PGE2-synthesizing capacity in hypothalamic endothelial cells, but not with the overall PGE2 production in the brain (Eskilsson et al., 2017), suggesting that local release of PGE2 to target hypothalamic neurons is critical for the hyperthermia-generating response. Taken together, these results indicate that cell signaling in endothelial cells in the brain is important for hyperthermia, possibly due to direct action of circulating LPS and/or cytokines.

In our previous study, we found that transient receptor potential vanilloid 1 (TRPV1) was highly expressed in astrocyte/tanycyte-like NSCs in the CVOs (Mannari et al., 2013). Moreover, activation of TRPV1 resulted in increased expression of Fos and STAT3 in astrocyte/tanycyte-like NSCs in the CVOs, as well as hypothermia (Mannari et al., 2013; Yoshida et al., 2016). Therefore, Fos expression in astrocyte/tanycyte-like NSCs in the CVOs may be closely associated with thermoregulatory responses in the brain. The OVLT located at the anterior wall of the third ventricle was identified as a site of IL-1ß and TNF-α production in response to peripheral administration of LPS (Quan et al., 1997). As the OVLT is located close to the surrounding POA, diffusion of pyrogenic mediators to the thermosensitive structures may be possible. Moreover, i.c.v. administration of recombinant TNF-α and IL-6 was reported to cause hyperthermia (Dinarello, 2004). IL-6 is produced and released within the brain in response to peripheral administration of LPS and has central pyrogenic activity (Chai et al., 1999). The binding of IL-6 to the IL-6 receptor stimulates gp130-associated JAK kinases, which leads to the activation of STAT3 (Heinrich et al., 2003). Collectively, the present study suggests that TLR4, Fos, and STAT3 signaling in astrocyte/tanycyte-like NSCs of the CVOs functions as an antipyretic regulator to prevent excessive hyperthermia during LPS-induced inflammation.

Acknowledgments

This work was supported in part by Scientific Research Grants from the Japan Society for the Promotion of Science (16K07027). The hybridoma for the anti-PV-1 (MECA-32, Eugene C. Butcher) antibody was obtained from the DSHB developed under the auspices of the NICHD, and maintained by The University of Iowa, Iowa City, IA 52242.

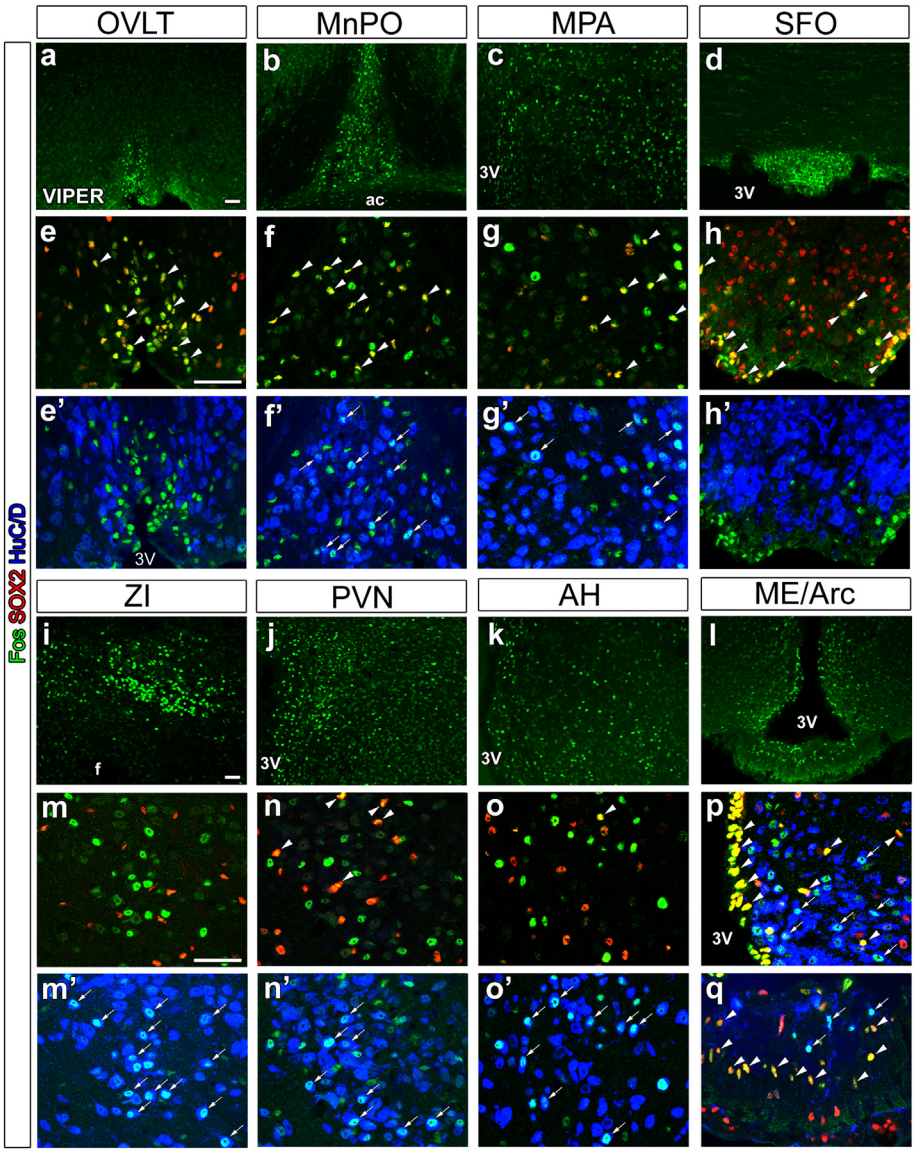

Fig. 15. Effects of i.c.v. administration of a high-dose TLR4 inhibitor, VIPER, on Fos expression in normal adult mice. Mice received i.c.v. administration of 1 mg/kg of VIPER and were sacrificed for Fos immunohistochemistry 2 h later. a-d, i-l: On low magnification, many Fos^+ nuclei were observed in several hypothalamic nuclei in addition to in the CVOs and Arc. e-h, e′-h′, m-q, m′-o′: In the CVOs, Fos^+ nuclei were frequently observed in $SOX2^+$ astrocyte/tanycyte-like NSCs (arrowheads) in the OVLT (e), SFO (h), and Arc (p), and in $SOX2^+$ astrocytes in the ME (q) and dorsal part of the Arc (p). Fos^+ nuclei were not observed in HuC/D^+ neurons (arrows) in the OVLT (e') or SFO (h′), but they were detected in the Arc (p) and ME (q). In other brain regions, Fos^+ nuclei were frequently observed in $SOX2^+$ astrocytes (arrowheads) and HuC/D^+ neurons (arrows) in the MnPO (f, f′), MPA (g, g′), and PVN (n, n′). In the ZI (m, m′) and AH (o, o′), Fos^+ nuclei were observed in HuC/D^+ neurons (arrows), but rarely in $SOX2^+$ astrocytes (arrowheads). Scale bars = 50 μm.

Appendix A. Supplementary data

Supplementary data to this article can be found online at https://doi.org/10.1016/j.jneuroim.2018.04.017.

References

Adcock, I.M., 1997. Transcription factors as activators of gene transcription: AP-1 and NF-kappa B. Monaldi Arch. Chest Dis. 52, 178–186.

Al-Saffar, H., Lewis, K., Liu, E., Schober, A., Corrigan, J.J., Shibata, K., Steiner, A.A., 2013. Lipopolysaccharide-induced hypothermia and hypotension are associated with inflammatory signaling that is triggered outside the brain. Brain Behav. Immun. 28, 188–195.

Banks, W.A., Robinson, S.M., 2010. Minimal penetration of lipopolysaccharide across the murine blood–brain barrier. Brain Behav. Immun. 24, 102–109.

Brasier, A.R., 2010. The nuclear factor-kappaB-interleukin-6 signalling pathway mediating vascular inflammation. Cardiovasc. Res. 86, 211–218.

Cao, C., Matsumura, K., Ozaki, M., Watanabe, Y., 1999. Lipopolysaccharide injected into the cerebral ventricle evokes fever through induction of cyclooxygenase-2 in brain endothelial cells. J. Neurosci. 19, 716–725.

Chai, Z., Gatti, S., Toniatti, C., Poli, V., Bartfai, T., 1999. Interleukin (IL)-6 gene expression in the central nervous system is necessary for fever response to lipopolysaccharide or IL-1ß: a study on IL-6-deficient mice. J. Exp. Med. 183, 311–316.

Chakravarty, S., Herkenham, M., 2005. Toll-like receptor 4 on nonhematopoietic cells sustains CNS inflammation during endotoxemia, independent of systemic cytokines. J. Neurosci. 25, 1788–1796.

Ching, S., Zhang, H., Belevych, N., He, L., Lai, W., Pu, X.A., Jaeger, L.B., Chen, Q., Quan, N., 2007. Endothelial-specific knockdown of interleukin-1 (IL-1) type 1receptor differentially alters CNS responses to IL-1 depending on its route of administration. J. Neurosci. 27, 10476–10486.

Chitravanshi, V.C., Kawabe, K., Sapru, H.N., 2016. Stimulation of the hypothalamic arcuate nucleus increases brown adipose tissue nerve activity via hypothalamic paraventricular and dorsomedial nuclei. Am. J. Physiol. Heart Circ. Physiol. 311, H433–H444.

Coats, S.R., Pham, T.T., Bainbridge, B.W., Reife, R.A., Darveau, R.P., 2005. MD-2 mediates the ability of tetra-acylated and penta-acylated lipopolysaccharides to antagonize *Escherichia coli* lipopolysaccharide at the TLR4 signaling complex. J. Immunol. 175, 4490–4498.

Conti, B., Tabarean, I., Andrei, C., Bartfai, T., 2004. Cytokines and fever. Front. Biosci. 9, 1433–1449.

Contreras, C., Nogueiras, R., Diéguez, C., Medina-Gómez, G., López, M., 2016. Hypothalamus and thermogenesis: heating the BAT, browning the WAT. Mol. Cell. Endocrinol. 438, 107–115.

Dinarello, C.A., 2004. Infection, fever, and exogenous and endogenous pyrogens: some concepts have changed. J. Endotoxin Res. 10, 201–222.

Eskilsson, A., Mirrasekhian, E., Dufour, S., Schwaninger, M., Engblom, D., Blomqvist, A., 2014. Immune-induced fever is mediated by IL-6 receptors on brain endothelial cells coupled to STAT3-dependent induction of brain endothelial prostaglandin synthesis. J. Neurosci. 34, 15957–15961.

Eskilsson, A., Matsuwaki, T., Shionoya, K., Mirrasekhian, E., Zajdel, J., Schwaninger, M., Engblom, D., Blomqvist, A., 2017. Immune-induced fever is dependent on local but not generalized prostaglandin E2 synthesis in the brain. J. Neurosci. 37, 5035–5044.

Furube, E., Morita, M., Miyata, S., 2015. Characterization of neural stem cells and their progeny in the sensory circumventricular organs of adult mouse. Cell Tissue Res. 362, 347–365.

Furube, E., Kawai, S., Inagaki, H., Takagi, S., Miyata, S., 2018. Brain region-dependent

heterogeneity and dose-dependent difference in transient microglia population increase during lipopolysaccharide-induced inflammation. Sci. Rep. 8, e2203.
Gay, N.J., Symmons, M.F., Gangloff, M., Bryant, C.E., 2014. Assembly and localization of toll-like receptor signalling complexes. Nat. Rev. Immunol. 14, 546–558.
Ghosh, S., May, M.J., Kopp, E.B., 1998. NF-kappa B and Rel proteins: evolutionarily conserved mediators of immune responses. Annu. Rev. Immunol. 16, 225–260.
Hayden, M.S., Ghosh, S., 2004. Signaling to NF-kappa B. Genes Dev. 18, 2195–2224.
Heinrich, P.C., Behrmann, I., Haan, S., Hermanns, H.M., Muller-Newen, G., Schaper, F., 2003. Principles of interleukin (IL)-6-type cytokine signalling and its regulation. Biochem. J. 374, 1–20.
Imamura, Y., Morita, S., Nakatani, N., Okada, K., Ueshima, S., Matsuo, O., Miyata, S., 2010. Tissue plasminogen activator and plasminogen are critical for osmotic homeostasis by regulating vasopressin secretion. J. Neurosci. Res. 88, 1995–2006.
Jann, B., Reske, K., Jann, K., 1975. Heterogeneity of lipopolysaccharides. Analysis of polysaccharide chain lengths by sodium dodecylsulfate polyacrylamide gel electrophoresis. Eur. J. Biochem. 60, 239–246.
Kelly, L., Bielajew, C., 1996. Short-term stimulation-induced decreases in brown fat temperature. Brain Res. 715, 172–179.
Laflamme, N., Rivest, S., 2001. Toll-like receptor 4: the missing link of the cerebral innate immune response triggered by circulating gram-negative bacterial cell wall components. FASEB J. 15, 155–163.
Laflamme, N., Lacroix, S., Rivest, S., 1999. An essential role of interleukin-1b in mediating NF-κB activity and COX-2 transcription in cells of the blood–brain barrier in response to a systemic and localized inflammation but not during endotoxemia. J. Neurosci. 19, 10923–10930.
Langlet, F., Mullier, A., Bouret, S.G., Prevot, V., Dehouck, B., 2013. Tanycyte-like cells form a blood-cerebrospinal fluid barrier in the circumventricular organs of the mouse brain. J. Comp. Neurol. 521, 3389–3405.
Lawrence, T., 2009. The nuclear factor NF-kB pathway in inflammation. Cold Spring Harb. Perspect. Biol. 1, a001651.
Lazarus, M., Yoshida, K., Coppari, R., Bass, C.E., Mochizuki, T., Lowell, B.B., Saper, C.B., 2007. EP3 prostaglandin receptors in the median preoptic nucleus are critical for fever responses. Nat. Neurosci. 10, 1131–1133.
Lee, D.A., Bedont, J.L., Pak, T., Wang, H., Song, J., Miranda-Angulo, A., Takiar, V., Charubhumi, V., Balordi, F., Takebayashi, H., Aja, S., Ford, E., Fishell, G., Blackshaw, S., 2012. Tanycytes of the hypothalamic median eminence form a diet-responsive neurogenic niche. Nat. Neurosci. 15, 700–702.
Lu, B., Antoine, D.J., Kwan, K., Lundback, P., Wahamaa, H., Schierbeck, H., Robinson, M., Van Zoelen, M.A., Yang, H., Li, J., Erlandsson-Harris, H., Chavan, S.S., Wang, H., Andersson, U., Tracey, K.J., 2014. JAK/STAT1 signaling promotes HMGB1 hyperacetylation and nuclear translocation. Proc. Natl. Acad. Sci. U. S. A. 111, 3068–3073.
Lysakova-Devine, T., Keogh, B., Harrington, B., Nagpal, K., Halle, A., Golenbock, D.T., Monie, T., Bowie, A.G., 2010. Viral inhibitory peptide of TLR4, a peptide derived from vaccinia protein A46, specifically inhibits TLR4 by directly targeting MyD88 adaptor-like and TRIF-related adaptor molecule. J. Immunol. 185, 4261–4271.
Maguire, O., Collins, C., O'Loughlin, K., Miecznikowski, J., Minderman, H., 2011. Quantifying nuclear p65 as a parameter for NF-κB activation: correlation between ImageStream cytometry, microscopy, and Western blot. Cytometry A. 79, 461–469.
Mannari, T., Morita, S., Furube, E., Tominaga, M., Miyata, S., 2013. Astrocytic TRPV1 ion channels detect blood-borne signals in the sensory circumventricular organs of adult mouse brains. Glia 61, 957–971.
McCusker, R.H., Kelley, K.W., 2013. Immune-neural connections: how the immune system's response to infectious agents influences behavior. J. Exp. Biol. 216, 84–98.
Miyata, S., 2017. Advances in understanding of structural reorganization in the hypothalamic neurosecretory system. Front. Endocrinol. 8, e275.
Miyata, S., Morita, S., 2011. A new method for visualization of endothelial cells and extravascular leakage in adult mouse brain using fluorescein isothiocyanate. J. Neurosci. Meth. 202, 9–16.
Miyata. S, 2015. New aspects in fenestrated capillary and tissue dynamics in the sensory circumventricular organs of adult brains. Front. Neurosci. 9, 390.
Morita, S., Miyata, S., 2012. Different vascular permeability between the sensory and secretory circumventricular organs of adult mouse brain. Cell Tissue Res. 349, 589–603.
Morita, S., Furube, E., Mannari, T., Okuda, H., Tatsumi, K., Wanaka, A., Miyata, S., 2016. Heterogeneous vascular permeability and alternative diffusion barrier in sensory circumventricular organs of adult mouse brain. Cell Tissue Res. 363, 497–511.
Mullarkey, M., Rose, J.R., Bristol, J., Kawata, T., Kimura, A., Kobayashi, S., Przetak, M., Chow, J., Gusovsky, F., Christ, W.J., Rossignol, D.P., 2003. Inhibition of endotoxin response by e5564, a novel toll-like receptor 4-directed endotoxin antagonist. J. Pharmacol. Exp. Ther. 304, 1093–1102.
Murray, C.L., Skelly, D.T., Cunningham, C., 2011. Exacerbation of CNS inflammation and neurodegeneration by systemic LPS treatment is independent of circulating IL-1β and IL-6. J. Neuroinflammation 8, 50.
Nakamura, K., 2011. Central circuitries for body temperature regulation and fever. Am. J. Physiol. Regul. Integr. Comp. Physiol. 301, R1207–R1228.
Nakano, Y., Furube, E., Morita, S., Wanaka, A., Nakashima, T., Miyata, S., 2015. Astrocytic TLR4 expression and LPS-induced nuclear translocation of STAT3 in the sensory circumventricular organs of adult mouse brain. J. Neuroimmunol. 278, 144–158.
Nilsson, A., Wilhelms, D.B., Mirrasekhian, E., Jaarola, M., Blomqvist, A., Engblom, D., 2016. Inflammation-induced anorexia and fever are elicited by distinct prostaglandin dependent mechanisms, whereas conditioned taste aversion is prostaglandin independent. Brain Behav. Immun. S0889-1591, 30549.
Oka, T., Oka, K., Kobayashi, T., Sugimoto, Y., Ichikawa, A., Ushikubi, F., Narumiya, S., Saper, C.B., 2003. Characteristics of thermoregulatory and febrile responses in mice deficient in prostaglandin EP1 and EP3 receptors. J. Physiol. 551, 945–954.
Park, S.E., Dantzer, R., Kelley, K.W., McCusker, R.H., 2011. Central administration of insulin-like growth factor-I decreases depressive-like behavior and brain cytokine expression in mice. J. Neuroinflammation 8, 12.
Paxinos, G., Franklin, K.B.J., 2001. The Mouse Brain in Stereotaxic Coordinates: Second Edition. Academic Press, San Diego.
Perkins, N.D., 2007. Integrating cell-signalling pathways with NF-κB and IKK function. Nature Rev. Mol. Cell Biol. 8, 49–62.
Quan, N., Whiteside, M., Kim, L., Herkenham, M., 1997. Induction of inhibitory factor kappa B alpha mRNA in the central nervous system after peripheral lipopolysaccharide administration: an in situ hybridization histochemistry study in the rat. Proc. Natl. Acad. Sci. U. S. A. 94, 10985–10990.
Ramachandran, G., 2014. Gram-positive and gram-negative bacterial toxins in sepsis: a brief review. Virulence 5, 213–218.
Rivest, S., 2003. Molecular insights on the cerebral innate immune system. Brain Behav. Immun. 17, 13–19.
Robins, S.C., Stewart, I., McNay, D.E., Taylor, V., Giachino, C., Goetz, M., Ninkovic, J., Briancon, N., Maratos-Flier, E., Flier, J.S., Kokoeva, M.V., Placzek, M., 2013. α-Tanycytes of the adult hypothalamic third ventricle include distinct populations of FGF-responsive neural progenitors. Nat. Commun. 4, e2049.
Rodríguez, E.M., Blázquez, J.L., Guerra, M., 2010. The design of barriers in the hypothalamus allows the median eminence and the arcuate nucleus to enjoy private milieus: the former opens to the portal blood and the latter to the cerebrospinal fluid. Peptides 31, 757–776.
Romanovsky, A.A., Steiner, A.A., Matsumura, K., 2006. Cells that trigger fever. Cell Cycle 5, 2195–2197.
Roth, J., Harré, E.M., Rummel, C., Gerstberger, R., Hübschle, T., 2004. Signaling the brain in systemic inflammation: role of sensory circumventricular organs. Front. Biosci. 9, 290–300.
Rummel, C., Hübschle, T., Gerstberger, R., Roth, J., 2004. Nuclear translocation of the transcription factor STAT3 in the guinea pig brain during systemic or localized inflammation. J. Physiol. 557, 671–687.
Rummel, C., Voss, T., Matsumura, K., Korte, S., Gerstberger, R., Roth, J., Hübschle, T., 2005. Nuclear STAT3 translocation in guinea pig and rat brain endothelium during systemic challenge with lipopolysaccharide and interleukin-6. J. Comp. Neurol. 491, 1–14.
Rummel, C., Sachot, C., Poole, S., Luheshi, G.N., 2006. Circulating interleukin-6 induces fever through a STAT3-linked activation of COX-2 in the brain. Am. J. Phys. 291, R1316–R1326.
Shammah-Lagnado, S.J., Negrão, N., Ricardo, J.A., 1985. Afferent connections of the zona incerta: a horseradish peroxidase study in the rat. Neuroscience 15, 109–134.
Sisó, S., Jeffrey, M., González, L., 2010. Sensory circumventricular organs in health and disease. Acta Neuropathol. 120, 689–705.
Steiner, A.A., Chakravartym, S., Rudaya, A.Y., Herkenham, M., Romanovsky, A.A., 2006. Bacterial lipopolysaccharide fever is initiated via toll-like receptor 4 on hematopoietic cells. Blood 107, 4000–4002.
Takeda, K., Akira, S., 2004. TLR signaling pathways. Semi. Immunol. 16, 3–9.
Vargas-Caraveo, A., Sayd, A., Maus, S.R., Caso, J.R., Madrigal, J.L.M., García-Bueno, B., Leza, J.C., 2017. Lipopolysaccharide enters the rat brain by a lipoprotein-mediated transport mechanism in physiological conditions. Sci. Rep. 7, 13113.
Wilhelms, D.B., Kirilov, M., Mirrasekhian, E., Eskilsson, A., Kugelberg, U.Ö., Klar, C., Ridder, D.A., Herschman, H.R., Schwaninger, M., Blomqvist, A., Engblom, D., 2014. Deletion of prostaglandin E2 synthesizing enzymes in brain endothelial cells attenuates inflammatory fever. J. Neurosci. 34, 11684–11690.
Yoshida, A., Furube, E., Mannari, T., Takayama, Y., Kittaka, H., Tominaga, M., Miyata, S., 2016. TRPV1 is crucial for proinflammatory STAT3 signaling and thermoregulation-associated pathways in the brain during inflammation. Sci. Rep. 6, 26088.
Yu, L., Wang, L., Chen, S., 2014. Endogenous toll-like receptor ligands and their biological significance. J. Cell. Mol. Med. 14, 2592–2603.